Environmental Radioactivity

F56

Institut für Umweltphysik (IUP), Universität Heidelberg

Im Neuenheimer Feld 229, 69120 Heidelberg

Version 1, April 2024

Revised by I. Levin and S. Preunkert

(Please sent any correspondence concerning this document to:
Susanne.Preunkert@iup.uni-heidelberg.de)

Summary

The experiment shall give an introduction into measurement techniques of (natural) radioactivity and provide insight into the application of radioactive isotopes as tracers in environmental research. Soil cores are collected and analysed for their natural (^{226}Radium) and artificial (^{137}Cesium fallout from the Chernobyl accident) radioactivity by low-level γ-spectroscopy. The exhalation rate of ^{222}Radon from the soil surface is measured using α-spectrometry and compared to theoretical estimates, which will be based on measured soil properties (^{226}Radium, soil texture and soil moisture).

1 Introduction and Motivation

1.1 Natural and artificial radioactivity

Naturally produced radio isotopes can be separated into two groups: The *primordial nuclides* have been produced during the formation of our planetary system by nucleosynthesis. Their radioactive half-lives ($T_{1/2}$) are of order 10^9 years. Prominent examples are ^{40}Potassium ($T_{1/2}$ = 1.28 10^9 years), ^{232}Thorium ($T_{1/2}$ = 1.4 10^{10} years), ^{235}Uranium ($T_{1/2}$ = 7.04 10^8 years) and ^{238}Uranium ($T_{1/2}$ = 4.47 10^9 years). ^{40}Ka decays into stable ^{40}Argon, but Uranium and Thorium continuously produce further radioactive isotopes, such as ^{222}Radon and ^{220}Radon. These secondary isotopes are called radiogenic.

The second group of radio isotopes are the so-called *cosmogenic* radio nuclides. They are produced through interaction of high-energy particles (cosmic radiation) mainly with atoms of the Earth atmosphere. Primary cosmic radiation is attenuated by the magnetic fields of the sun and the Earth. The production rate of cosmogenic radio nuclides therefore changes with changes of these magnetic fields. Prominent examples of cosmogenic isotopes are Radiocarbon (^{14}C: $T_{1/2}$ = 5700 years), Tritium (^{3}H: $T_{1/2}$ = 10.3 years), ^{7}Beryllium ($T_{1/2}$ = 53.5 days) and ^{10}Beryllium ($T_{1/2}$ = 1.5 10^6 years).

A third important group of radioactive isotopes in our environment are artificially produced, e.g. during nuclear energy production. They are released to the environment mainly during reprocessing of nuclear waste. Prominent examples are ^{85}Krypton ($T_{1/2}$ = 10.8 years), ^{131}Iodine ($T_{1/2}$ = 8 days) and ^{137}Cesium ($T_{1/2}$ = 30.2 years).

Many of the natural and artificially produced radioactive isotopes are important due to their role as tracers in the environment, either due to their particular distribution of sources and sinks or for dating purposes. With half-life times between days and centuries, their small (activity) concentrations can be rather easily measured via their radioactive decay. Nuclides with very long lifetimes are, however, today often more accurately measured via (accelerator) mass spectrometry (e.g. ^{10}Be but also ^{14}C). These isotopes will not be tackled in this exercise. Here we will focus on the measurement of ^{137}Cs and ^{226}Ra with low-level γ-spectroscopy as well as ^{222}Rn with α-spectrometry.

1.2 The importance of natural radio isotopes for human population

Natural radioactive isotopes contribute about 80% to the public radiation exposure (Fig. 1). Most important in this regard is the radioactive noble gas radon (and its progenies), formed as ^{222}Radon and ^{220}Radon (Thoron) from decay of radium isotopes, elements of the Uranium-Thorium series and constituents of all natural soils. As a noble gas radon can escape from the unsaturated soil into the atmosphere, where it decays by α-decay with a half-life time of 55.6 seconds (^{220}Radon) respectively 3.8 days (^{222}Radon) into short-lived radio-isotopes that are quickly attached to aerosols (Fig. 2).

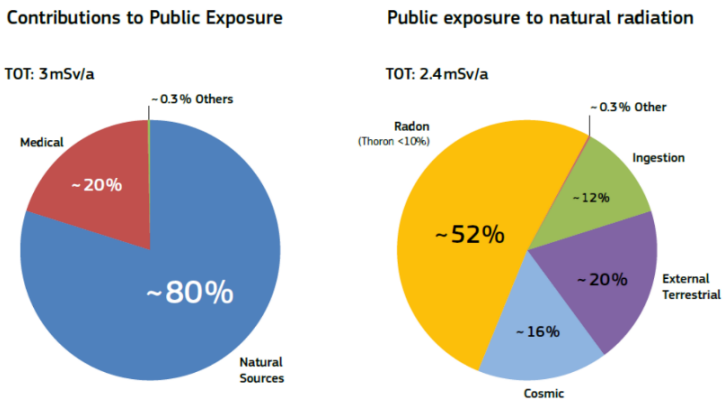

Figure 1: Contributions of radioactivity to public exposure (from Cinelli et al., 2019)

Radon isotopes are responsible for more than 50% of public exposure to natural radiation. Radon diffusion from the ground into basements of houses increase indoor radon activity concentrations and can contribute to large radiation exposure. About 5% of the lung cancer risk in Germany is attributable to indoor radon (Wichmann et al., 2006). Therefore, indoor radon has increasingly been subject to safety regulations for protection against ionizing radiation (EU, 2013) and so-called Radon Prone/Priority Areas (RPA) must be identified (see e.g. Bossew, 2018).

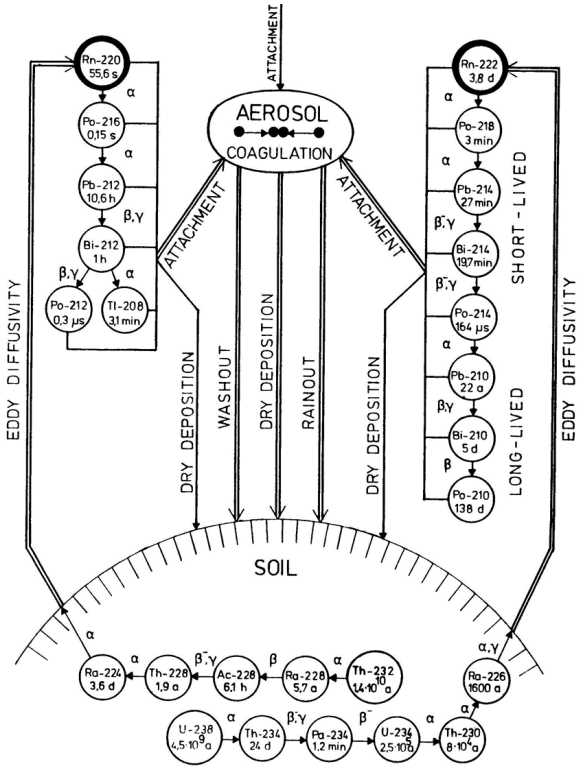

Figure 2: ^{222}Radon and ^{220}Radon and their decay products in the open atmosphere (from Porstendörfer 1994)

1.3 The contribution of artificial radioactivity on human population

Not only natural radioactivity is contributing to our every-day radiation exposure: Since many decades, the increasing energy demand of modern civilisation has been covered by a significant share of (supposedly) climate-friendly nuclear energy production. However, similar to the use of fossil fuels, which, through increasing emissions of the greenhouse gas carbon dioxide (CO_2) is leading to anthropogenic climate warming, utilisation of nuclear energy has also not been without negative consequences for our environment. A prominent example is the nuclear accident of Fukushima in Japan in March 2011, causing huge nuclear contamination with inhabitable areas in the vicinity of these reactors. Also the Chernobyl accident in the Ukraine in April 1986, caused immense radioactive fallout, mainly in eastern Europe, but also in the western parts of our continent. This did not only concern short-lived radio isotopes, such as ^{131}Iodine that mainly contributed to the radiation dose during and shortly after the accident, but there still remain measurable amounts of the released long-lived ^{137}Cesium isotope in the upper layers of soils, also in our region around Heidelberg (Fig. 3).

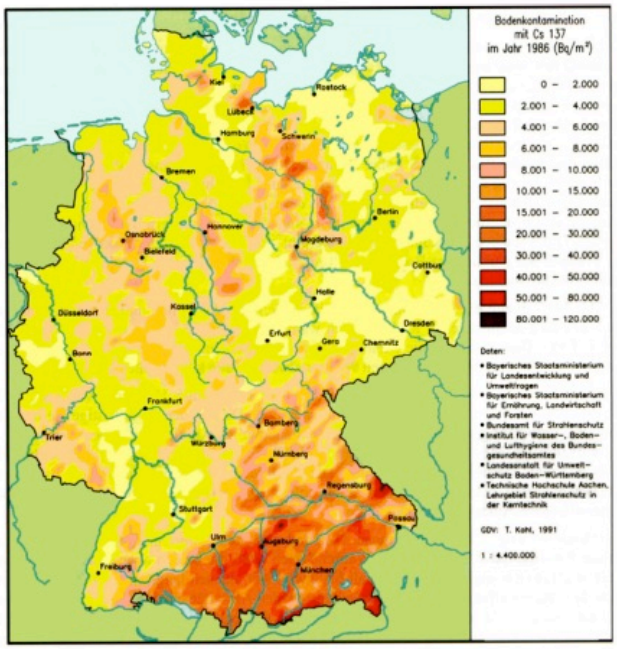

Figure 3: Deposition of ^{137}Cesium in Germany released during the Chernobyl reactor accident in April 1986 (Strahlenschutzkommission 2006)

1.4 Aims of the exercise

In this exercise soil cores are collected and analysed for their static physical properties, which are soil porosity, grain size distribution as well as ^{226}Radium and ^{137}Cesium activity concentrations using low-level γ-spectroscopy. The aims are to estimate the ^{137}Cs fallout from the Chernobyl accident at the location of the core. The ^{226}Ra activity concentration in the soil, together with the physical parameters of the soil and measured soil moisture form the basis to calculate the ^{222}Radon flux from the soil surface to the atmosphere. This process-based ^{222}Radon flux is compared with direct flux measurements close to the location of soil core sampling. Two chamber systems are used, one automatic so-called AutoFlux instrument (see Appendix B1) that is permanently installed in the Botanic Garden and one manual system. Both are measuring the ^{222}Radon released from the soil surface by α-spectrometry with ionisation chamber (AutoFlux) and with a surface barrier detector (RAD7, see Appendix B2).

As the topics covered in this exercise reach from pure experimental physics to special applications in Environmental Physics, a rather comprehensive introduction on basic derivations is provided below and in the respective references. Additional literature on particular topics for further reading is listed below.

Gamma spectrometry:

Gilmore, G., und Hemingway, H., 1995. Practical gamma-ray spesctrometry. John Wiley and sons, Chichester, England.

Radio nuclides as tracers in the environment:

Fröhlich, K., 2010. Environmental Radionuclides: Tracers and Timers of Terrestrial Processes. In: Radioactivity in the Environment, Volume 16, Elsevier Verlag.

Schery, S., 2001. Understanding radioactive aerosols and their measurement. Kluwer Academic Publishers, Dordrecht, Netherlands.

Radioactivity and radiation protection:
Cinelli, G., De Cort, M. & Tollefsen, T. (Eds): European Atlas of Natural Radiation, ISBN 978-92-76-08259-0, https://data.europa.eu/doi/10.2760/46388, 2019.
Grupen, C., Grundkurs Strahlenschutz, Vieweg Verlag, 2000.

2 Theoretical Background

2.1 Radioactive decay

From the known ca. 2500 nuclides only about 270 are stable (Faure and Mensing, 2005); therefore, from a nuclear physics perspective, radioactivity can be seen as the normal status. The number of decaying radio nuclides per time interval dt is proportional to the number nuclides N, with λ being the radioactive decay constant:

$$dN(t) = -\lambda N(t)dt \quad (1).$$

Solving this differential equation yields the radioactive decay law

$$N(t) = N_0 e^{-\lambda t} \quad (2).$$

The decay constant is the inverse time (radioactive lifetime τ) in which the starting concentration N_0 decreased to 1/e. Inserting the half lifetime $T_{1/2}$ into Eq. 2 yields the following expression for λ

$$N\left(T_{\frac{1}{2}}\right) = \frac{N_0}{2} = N_0 e^{-\lambda T_{1/2}} \quad \rightarrow \quad \lambda = \frac{\ln(2)}{T_{1/2}} = \frac{1}{\tau} \quad (3).$$

The activity of a sample A(t) is equal to the number nuclei, which decay within the time interval t

$$A(t) = -\frac{dN}{dt} = \lambda N(t) = \frac{N(t)}{\tau} \quad (4).$$

A(t) of a sample can be calculated from the decay constant (or radioactive lifetime) and the number of nuclei in the sample. The SI activity unit is Becquerel (1 Bq = 1 decay per second). The unit Curie (1 Ci = activity of one g of radium = 3.7 10^{10} Bq) is only found in old literature.

To estimate the effect of radiation on living organisms, not only the activity is important, therefore the following quantities have been defined: The **absorbed dose** (D) is a dose quantity, which is the measure of the energy deposited in matter by ionizing radiation per unit mass. Its unit is Gray (Gy) or

in SI units Joule/kg (J/kg). As the absorbed dose does not tell about the effect of the absorbed radiation on living organisms, the **equivalent dose** (H) has been introduced. It is derived from the physical quantity absorbed dose, but also takes into account the biological effectiveness of the radiation, which is dependent on the radiation type and energy. It has also the SI unit J/kg, but is measured in Sievert (Sv) and calculated from D by multiplication with a radiation weighting factor w that represents the relative biological effectiveness of the radiation and modifies the absorbed dose to take account of the different biological effects of various types and energies of radiation.

$$H[Sv] = \mathrm{w} \cdot \mathrm{D}[Gy] \qquad (5).$$

The weighting factors w of different radiation types are defined by regulation (see Wikipedia: https://en.wikipedia.org/wiki/Equivalent_dose). An estimate of the equivalent dose of a radioactive point source (in this exercise we use an ^{152}E source, see Sec. 4.2.1) is possible using a nuclide-specific dose constant Λ ([Λ] = mSv m^2 h^{-1} GBq^{-1})

$$H[Sv] = \frac{\Lambda \cdot activity}{distance^2}\ \mathrm{t} \qquad (6).$$

For many radio isotopes the equivalent dose rate can be calculated e.g. at http://www.radprocalculator.com/Gamma.aspx.

2.2 Radon production in the soil and its transport into the atmosphere

2.2.1 Radon production in soil

The basic assumptions and parameterizations of the radon production and its transport from the soil air into the atmosphere follow essentially the model description in Karstens et al. (2015) and Karstens and Levin (2023). These are summarized here for reference.

The production of radon gas in the soil is calculated according to Schüßler (1996).

$$Q(z) = \lambda\ \rho_b(z)\ c_{Ra}(z)\ \varepsilon(z) \qquad (7)$$

with radon source Q(z) [Bq m^{-3} s^{-1}], radon decay constant (λ = 2.0974 x 10^{-6} s^{-1}), soil bulk density ρ_b [kg m^{-3}], ^{226}Ra activity concentration in soil material c_{Ra} [Bq kg^{-1}], and emanation coefficient ε. The emanation coefficient ε is depending on soil texture (sand, silt, clay fraction), soil moisture, soil porosity and temperature as is reported in Zhuo et al. (2008). Here we do, however, follow Karstens et al. (2015) and use only constant emanation coefficients for the different soil fractions, i.e. ε_{sand} = 0.285 for sand, ε_{silt} = 0.382 for silt, and ε_{clay} = 0.455 for clay.

The unit volume of soil consists of the soil material fraction θ_m, the fraction that is filled with water θ_w, and the air-filled fraction θ_a so that

$$\theta_m + \theta_w + \theta_a = 1 \qquad (8).$$

The porosity θ_p of the soil is defined as $\theta_p = 1 - \theta_m = \theta_w + \theta_a$. Soil water saturation is thus defined as the ratio between volumetric soil moisture θ_w and soil porosity θ_p

$$S = \frac{\theta_w}{\theta_p} \quad (9).$$

2.2.2 Radon transport in the soil air and exhalation rate at the soil surface

The basic assumption of the radon flux model is that transport of radon in the soil and across the soil surface into the atmosphere occurs predominantly by molecular diffusion (Nazaroff, 1992) and can be described by Fick's first law

$$j(z) = -D_e \frac{\partial C(z)}{\partial z} \quad (10)$$

where j(z) is the radon flux, D_e the effective diffusion coefficient of radon in soil air, C the radon activity concentration and z the distance in vertical direction.

Together with the continuity equation for radon at steady state (no explicit time dependence assumed)

$$\frac{\partial j(z)}{\partial z} = = Q(z) - \lambda C(z) \quad (11)$$

and the boundary conditions of the radon concentration approaching zero at the soil-air interface and zero concentration gradient at great depth (cf. Fig. 4), the radon flux at the surface can be calculated by

$$j(z=0) = -Q\sqrt{\frac{D_e}{\lambda}} = -Q\,\bar{z} \quad (12)$$

where $\bar{z}$ is the diffusion length.

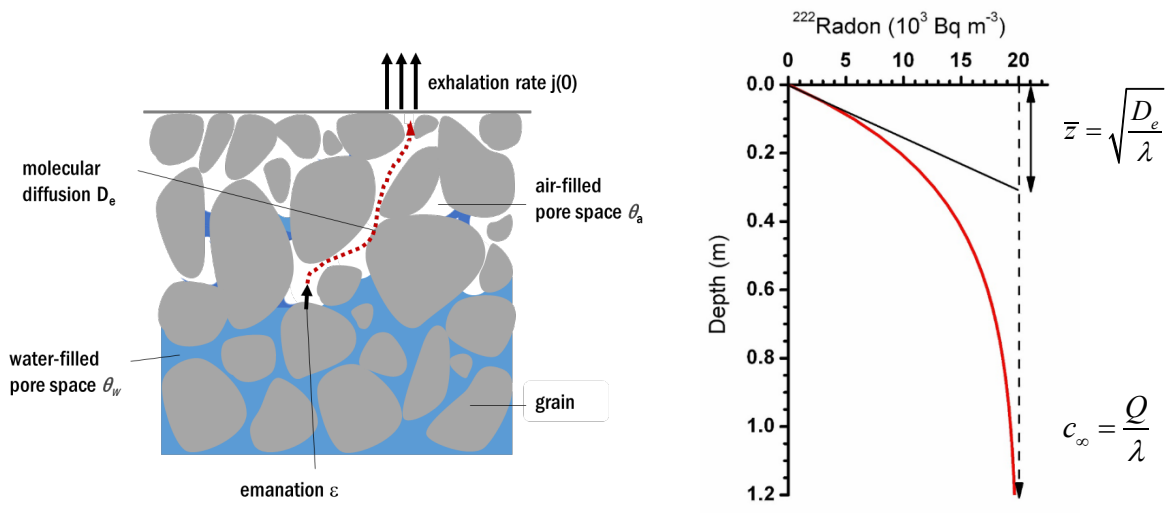

Figure 4, left: Sketch of the production and transport of ^{222}Radon from the soil grains to the atmosphere. Right: Theoretical profile of ^{222}Radon in soil air. If a profile of ^{222}Radon activity concentrations in soil air would be measured, the diffusion coefficient D_e could be determined from the diffusion length z according to Eq. 12, while the ^{222}Radon source strength Q could be estimated from the ^{222}Radon activity concentration at depths where the ^{222}Radon activity change with depth $\delta c/\delta z$ approaches zero (see Karstens et al., 2015).

2.2.3 Diffusion parameterization

As we are not measuring a ^{222}Radon profile in this exercise, we need to estimate D_e from (measured) soil properties: The effective diffusion of radon in the soil depends on the percentage of soil air volume available for gas diffusion and on the soil texture. We use the parameterization developed by Millington and Quirk (1960), which is based on soil porosity θ_p and volumetric soil moisture θ_w (referring to the total volume of the soil).

$$D_e = D_a \frac{(\theta_p - \theta_w)^2}{\theta_p^{\frac{2}{3}}} \quad (13)$$

where D_a=1.1 x 10^{-5} m^{-2} s^{-1} is the diffusion coefficient of radon in air. The temperature dependence of the effective diffusivity is taken into account according to Schery and Wasiolek (1998)

$$D_e = D_{e0} \left(\frac{T}{273}\right)^{\frac{2}{3}} \quad (14)$$

with soil temperature T [K] and effective diffusivity D_{e0} at temperature 273K.

2.3 Application of ^{222}Rn flux estimates in atmospheric studies

2.3.1 Distribution of the ^{222}Rn flux in Europe

Karstens and Levin (2023) estimated ^{222}Radon fluxes for Europe based on soil texture and uranium maps as well as on two different land surface model-based soil moisture estimates (ERA5-Land and GLDAS-Noah2.1) for Europe (for references of the input data sets, see Karstens and Levin, 2023). Figure 5 shows the two flux maps for March and July 2017 as well as the differences between the two estimates. It is obvious that there are large differences in the ^{222}Rn fluxes, which here solely result from the differences in the soil moisture estimates of the two land surface models.

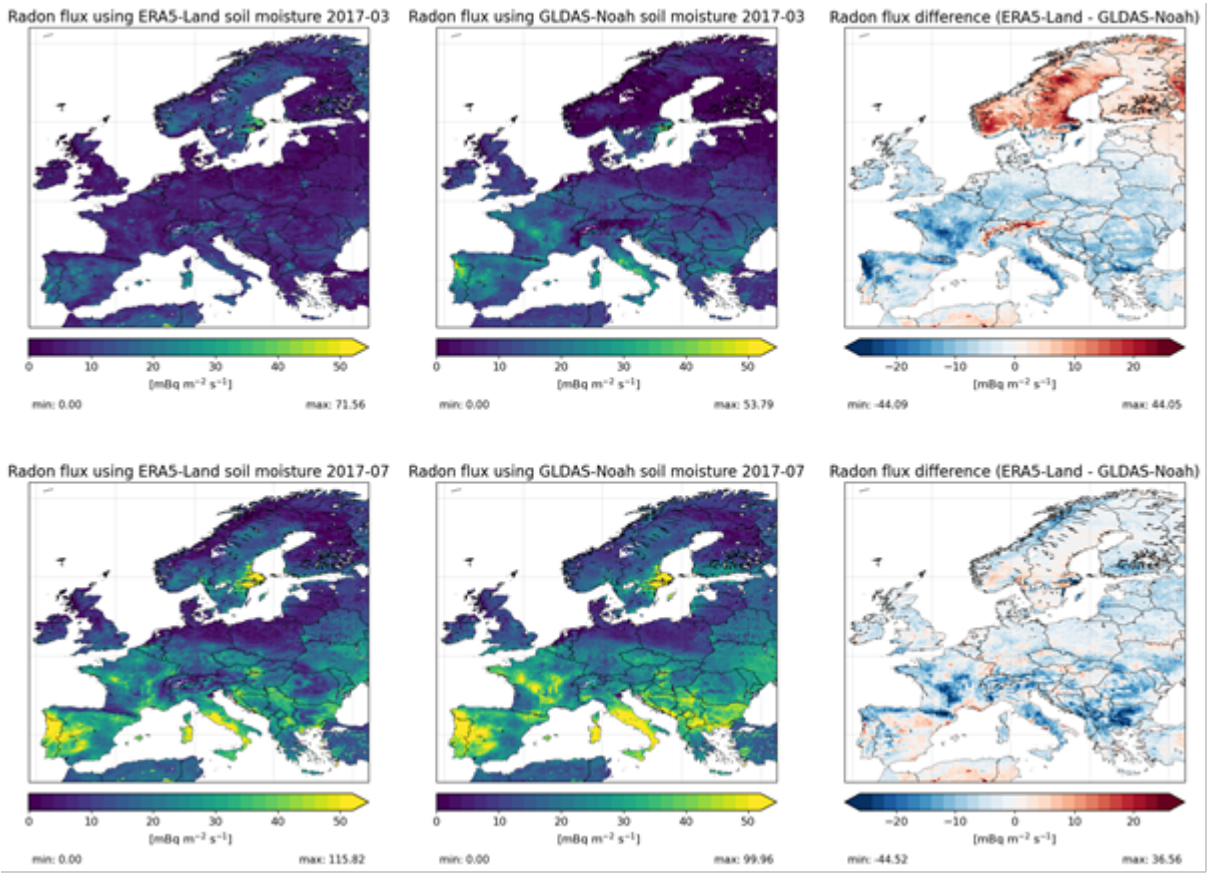

Figure 5: Monthly mean radon flux for March and July 2017 based on the ERA5-Land and GLDAS-Noah2.1 soil moisture reanalyses together with the difference between the two maps.

Based on our currently available information, it is hard to decide, which flux map is more realistic, because representative experimental data of soil moisture, but also of exhalation rates from the soil surface are sparse. Within this exercise we want to investigate the parameters governing the ^{222}Rn flux from soils and gain some insight into their uncertainties.

2.3.2 Radon as atmospheric transport tracer

Reliable estimates of the ^{222}Rn flux from soils are not only important to evaluate the contribution of radon and its progeny to the public radiation dose, but ^{222}Rn can also be used as a tracer for transport processes in the atmospheric Boundary Layer. The only source of ^{222}Rn to the atmosphere is its flux from the soil surface while its only sink (as a noble gas) is its well-known radioactive decay. The activity concentration of ^{222}Rn in the atmospheric Boundary Layer is thus determined by the soil flux and by turbulent mixing. If vertical mixing is suppressed close to the ground, e.g. during stable (night-time) conditions, ^{222}Rn can accumulate close to the ground, while during strong vertical convection conditions, e.g. during daytime in summer, emissions from the ground are quickly diluted in the vertical and activity concentrations close to the ground are low. The same is true for the concentration of other gases, such as methane or carbon dioxide, which have their sources also close to the ground. Figure 6 shows parallel measurements of ^{222}Radon and of the greenhouse gases (GHG) methane (CH_4) and carbon dioxide (CO_2) together with wind velocity on the roof of the former Institute für Umweltphysik in Heidelberg during 6 days in summer 1996. At low wind velocities in the last two days of the period we observe strong increases of all three gases during night and a fast decrease after sun rise. This diurnal variation is mainly caused by changes in atmospheric mixing conditions, which is the

reason for the good correlations of ^{222}Rn with each of the two GHGs (right panels of Fig. 6). Assuming similar homogeneous distribution of the GHG emissions as those of ^{222}Rn, we could make an estimate of their fluxes from the corresponding slopes of the regression lines if the ^{222}Rn flux were known (the Radon Tracer Method, see e.g. Levin et al., 1999; 2021).

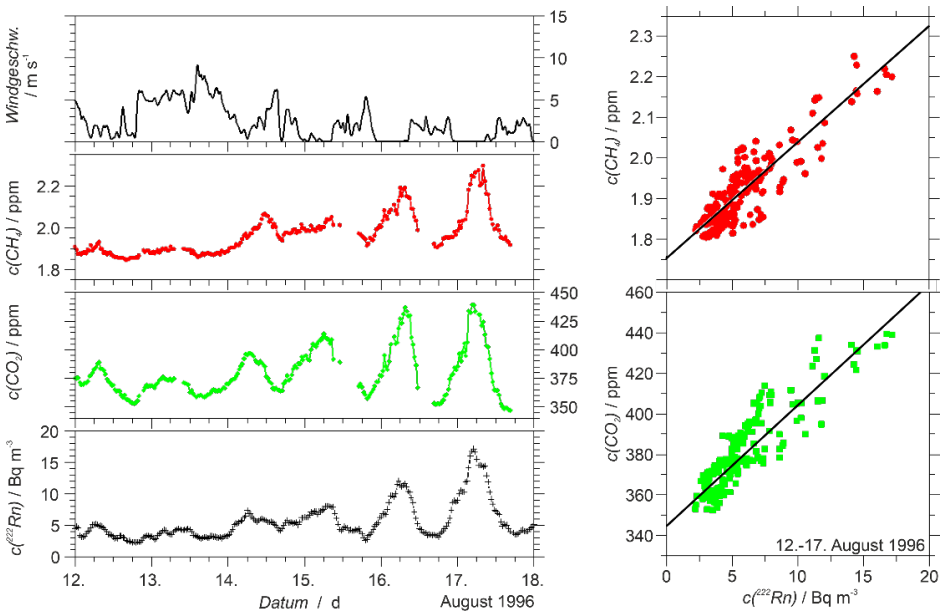

Figure 6: Temporal variation of atmospheric CH_4, CO_2 and ^{222}Radon measured on the roof of the old IUP building at INF 366 in Heidelberg together with wind velocity. The right hand side diagrams show the correlations between ^{222}Radon and CH_4 and CO_2 respectively. Multiplying the slopes of the regression lines with the mean ^{222}Radon flux from soils in the influence area of the IUP site would yield mean CH_4 or CO_2 fluxes.

3 Instrumentation

While long-lived radio isotopes such as ^{10}Be and also ^{14}C are quite often measured by sophisticated mass spectrometry, short-lived isotopes are rather easily detected by their radioactive decay. Depending on the nuclide, it is principally possible to measure their α- $\beta-$ or γ-radiation. Compared to γ- or α-radiation, detection by β-spectrometry is limited by the fact that the emitted β-particle is not characteristic of a particular element but it has a continuous spectrum, because the also emitted neutrino takes part of the decay energy with it. α- and γ-radiation have discrete spectra. However, α-particles have a rather short reach and can already be absorbed in the sample to be analysed (e.g. in a soil sample). In such cases chemical extraction of the element may be required. However, in the case of gas samples, α-spectrometry is a common technique e.g. for radon analysis in atmospheric or soil air. In the current exercise we will apply γ-spectroscopy for the ^{137}Cs and ^{226}Ra analysis on soil

samples and α-spectrometry for radon analysis of soil air resp. soil exhalation samples, and also for atmospheric measurements (e.g. Levin et al., 2002).

3.1 Low-level γ-spectroscopy

Interaction of γ-radiation with material occurs via three processes, depending on the energy of the radiation: Photoelectric effect, Compton effect and pair production (cf. Fig. 7)

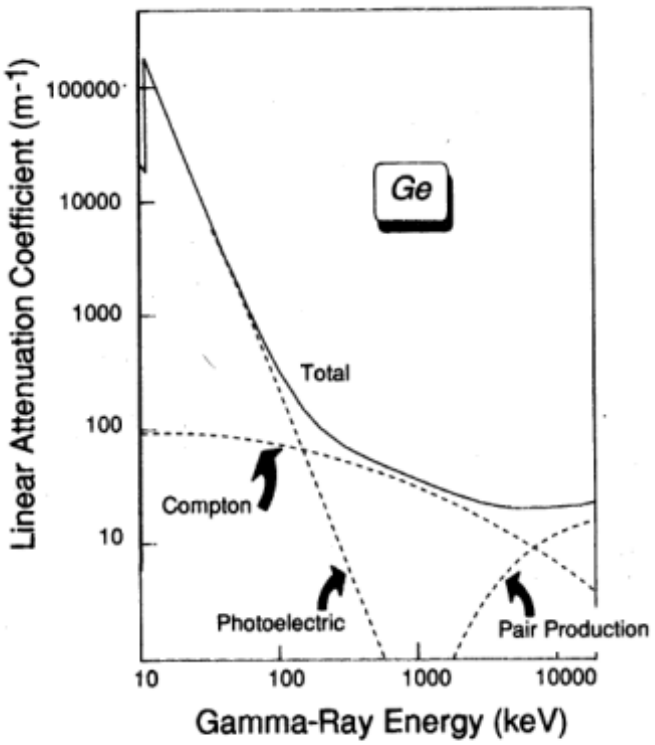

Figure 7: Interaction of γ-radiation with Germanium (from Gilmore, 1995)

Photoelectric effect: During the photoelectric effect the entire γ-energy (frequency ν) is transferred to an electron of an atom in the target, which leaves the atom with a kinetic energy E_{kin} (E_b = binding energy)

$$E_{kin} = h\nu - E_b \tag{15}$$

Compton effect: During the Compton effect the γ-quant hits an electron and transfers only part of its energy. The γ-quant changes its energy E_γ depending on the scattering angle θ

$$E'_\gamma = \frac{E_\gamma}{(1+\epsilon\,(1-\cos\theta))} \tag{16}$$

where $\epsilon = \frac{E_\gamma}{m_e c^2}$.

Pair production: At high energy of the γ-quant it can produce an electron – positron pair.

3.2 Principal setup of low-level γ-spectroscopy

For the detection of γ-radiation we can use scintillation (e.g. NaI) or semiconductor detectors. At the beginning of γ-spectroscopy mainly silicate detectors have been used. These have subsequently been replaced by Lithium-drifted cooled Germanium detectors (Ge(Li)) and finally by High-Purity Germanium (HP Ge) and other detector types. In the following, the individual components of the measurement system are described (cf. Fig. 8).

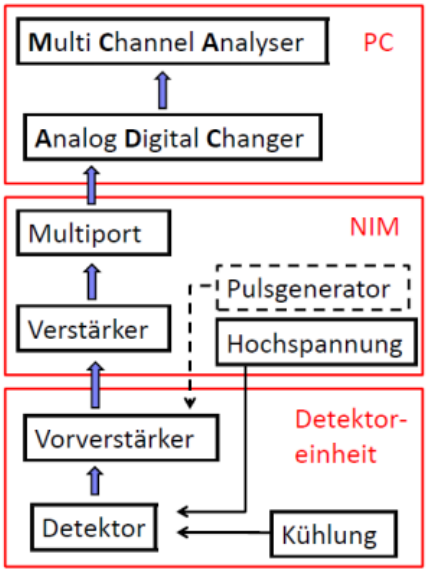

Figure 8: Sketch of the low-level γ-spectroscopy system as used in this exercise. The Multi-Channel Analyser (MCA) and Analog Digital Converter (ADC) are mounted in the Multiport but are controlled by the PC.

3.2.1 Detector

The detector types used in this exercise are High Purity Germanium semiconductor detectors. From their principle, these are diodes, which are operated in reverse direction with a very thick transfer zone. If a γ-quant passes through this active zone, electron-hole pairs (an electrical signal) are generated. The number of free electron-hole pairs and therewith the size of the electrical signal depends on the energy of the γ-quant.

Germanium is better suited as detector material than Siliceous, as it has a higher atomic number and thus good absorption characteristics. A small band width between conduction and valence band as well as practical reasons, such as availability of the material, are also relevant. The energy of 3.0 eV is required to generate an electron-hole pair in Germanium (Schery, 2001). The γ-quant of a 662 keV (^{137}Cs) decay will thus produce about 2.2 10^5 free electron-hole pairs. As the mean free path length of γ-radiation is rather large, the active zone of the detector should be as large as possible, in order to yield high efficiency. Germanium detectors for γ-spectroscopy should, therefore, principally be as large as possible. The electrical field for such a large geometry therefore often reaches voltages of several thousand volts (Schery, 2001). In order to minimize corresponding leak currents during their operation (the gap between valence and conduction band for Germanium is only 0.7 eV), Germanium detectors are cooled with liquid nitrogen (-196°C). In order to avoid water condensation on the

detector, its housing is evacuated (Fig. 9). The most important pre-requisites for low-level γ-spectroscopy are the following:

- A detector window as thin as possible but vacuum-tight -> Beryllium or Carbon
- An energy resolution as high as possible -> no mechanical vibrations, cooling of electronics
- Low radioactive background -> use material with little own radioactivity, protection with lead or cupper.

Since the development of semi-conductor γ-spectroscopy a number of different geometries of the detector crystal have been developed with different advantages and disadvantages; the geometry needs to be adjusted to the individual measurement situations (i.e. energy of the γ-radiation, sample size, activity range to be measured). Contrary to α-spectrometry (see below), shielding of γ-detectors with lead is required, as γ-radiation from the immediate surroundings (e.g. by ^{40}Ka) would lead to a huge detector background. Secondary γ-radiation by lead is further shielded by an inner cupper surface.

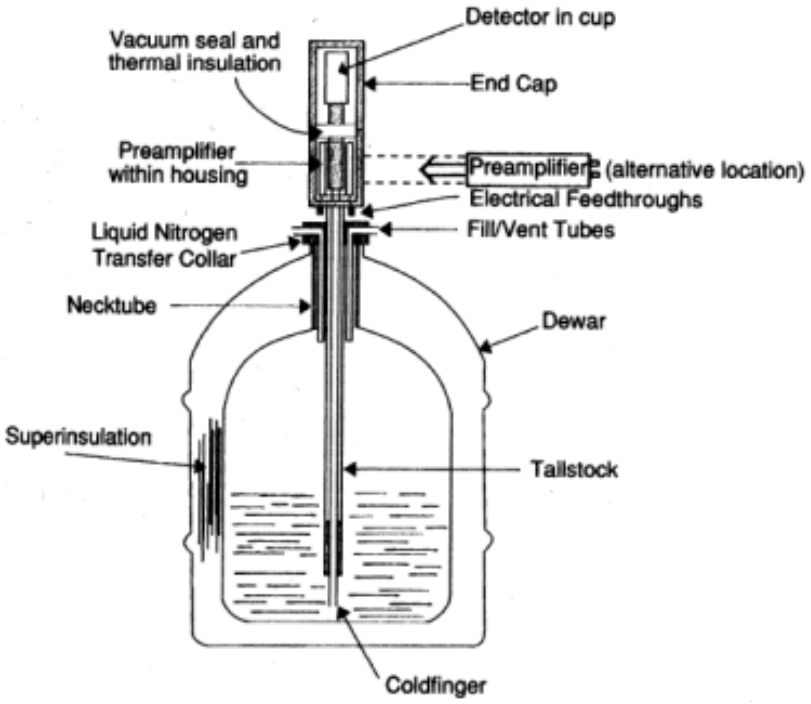

Figure 9: Principal setup of a low-level γ-detector (from Gilmore, 1995)

In this exercise we use two different HP Ge γ-detector types:

1. A p-type Germanium Planar detector (Type PGP2010, Ser. No. G151 from Detector Systems GmbH, named DSG detector in the lab). It is suited for γ-energies down to a few keV, but has rather bad efficiency.

2. An Intrinsic Germanium Coaxial detector (Type IGC22, Ser. No. DI-220 from Princeton Gamma-Tech GmbH, named PGT detector in the lab). It has relatively high efficiency but is not suited for low γ-energies.

The DSG detector is used for ^{226}Radium progeny measurement while we use the PGT detector for ^{137}Cesium profile measurement. As the direct γ-radiation from ^{226}Ra decay has a low energy (186.21 keV), which overlaps with the 185.72 keV line from ^{235}U decay, we measure ^{226}Ra via its progeny ^{214}Pb and ^{214}Bi. For this the soil sample is stored for more than 23 days (> 6 half-life times of ^{222}Rn) in an air-tight analysis container in order not to lose any ^{222}Rn during equilibration of all its progeny before analysis. The γ-spectrum of a soil sample collected close to Heidelberg with the peaks evaluated for the specific ^{226}Ra activity estimation marked in red is shown in Fig. 10.

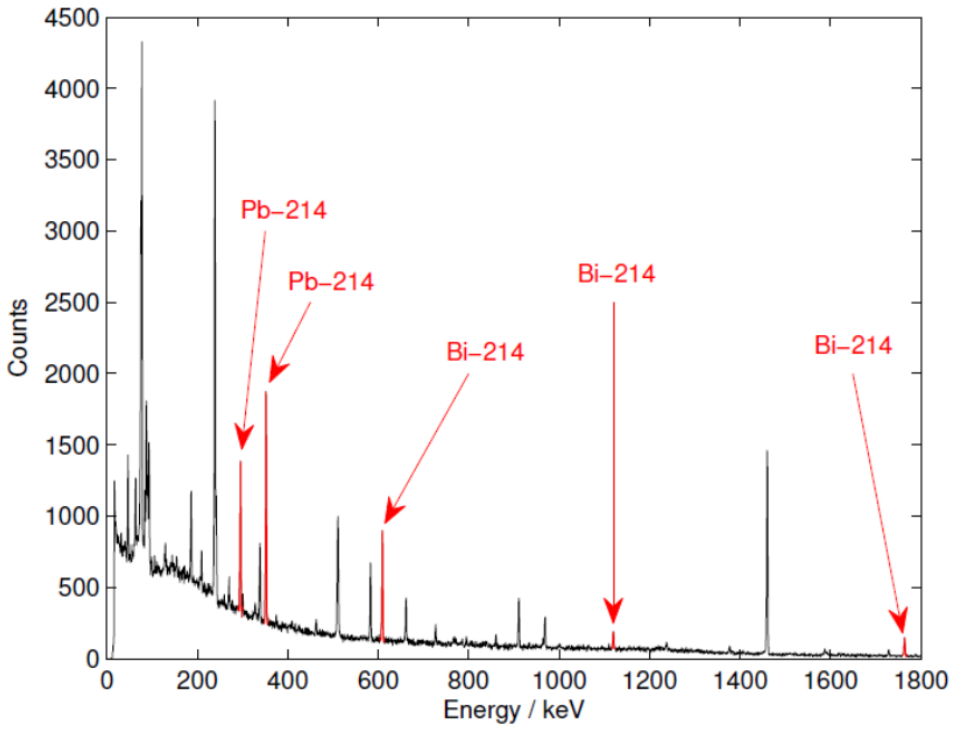

Figure 10: Typical γ-Spectrum of a soil sample with the 5 peaks from its progeny used for ^{226}Ra activity estimate marked in red (from Schwingshackl, 2013).

3.2.2 Pre-amplifier and amplifier

The 2.2 10^5 free electron-hole pairs from one ^{137}Cs decay correspond to an electrical signal of only 0.035 pC. This is why this primary signal needs to be amplified by a pre-amplifier to some 100 mV. The pre-amplifier integrates the signal from the detector and generates electrical pulses that are proportional to the original signal. It is thus important to suppress electronic noise by integrating the pre-amplifier in the detector cooling system (Fig. 9). The main amplifier amplifies the signal from the pre-amplifier to a 0-10 V electrical signal and transforms it into a Gaussian peak (Fig. 11). The electronic switching could lead to a so-called “under-shoot”. As this effect can diminish the energy resolution, it needs to be suppressed (“pole zero” on the amplifier board must be switched on).

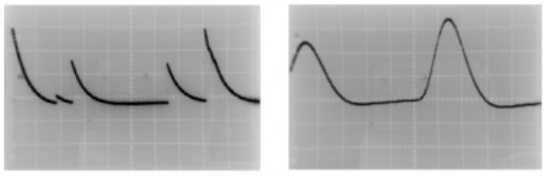

Figure 11: Characteristic signal before (left) and after (right) the main amplifier

3.2.3 Multiport, Analog Digital Converter (ADC) and Multi-Channel Analyser (MCA)

The role of the multiport in our system is to couple the detector(s) or amplifier(s) with the ADC. It hosts the ADC and the MCA (in German: Viel-Kanal-Analysator, VKA), both being controlled by the PC. The ADC transforms the analogous signal from the amplifier into a digital one, which is then stored in the different channels of the MCA. An upper (ULD) and a lower level discriminator (LLD) allow to select the energy range of the stored spectrum. While the ADC/MCA system processes a signal, no other signal can be counted; this time interval is called *dead-time* and depends on the activity of the sample. At high counting rates (e.g. with high noise counts) this time interval can be large. Therefore, it is important to suppress these noise counts, e.g. by increasing the LLD.

3.2.4 Interpretation of the γ-spectra

Although γ-radiation emitted during the decay of a particular nuclide has a well-defined energy, the resulting signal from the Ge crystal is seen not only at on energy channel. The main peak results from the γ-quants that lost their entire energy in the crystal (originating mainly from the photoelectric effect). Figure 12 from Gilmore (1995) illustrates the processes happening in the detector.

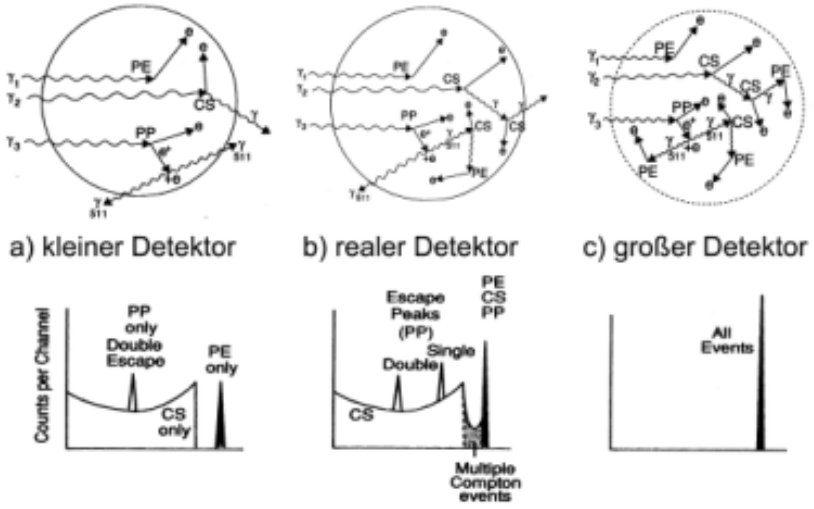

Figure 12: Model of the interaction of γ-radiation in a crystal in order to understand the structure of the γ-spectrum (lower panels). CS: Compton radiation, PE: photoelectric effect, PP: pair production

In an (un-realistically) large detector, the entire energy of a γ-quant is transferred into electron-hole pairs, no matter if the quant had lost some of its energy before, e.g. by inelastic scattering (Compton effect). This is because the interactions within the crystal are much faster than the integration of the electric signal(s). In this situation, we would indeed expect only one single peak per radio nuclide, the full energy peak. This is different in the case of a very small detector; here the γ-quant may leave the active zone after inelastic scattering. The remaining energy of the leaving γ-quant is thus missing in the detector signal and the count shows up somewhere below the Compton edge. In addition, the spectrum contains another peak at exactly 1022 keV (2 x electron mass of 511 keV) below the full energy peak (if E > 1022 keV) due to pair production where the positron hits an electron of the

detector material and both decay into 2 γ-quants of exactly 511 keV each (annihilation). A real detector behaves intermediate between the two extremes. In addition to the "double escape" peak we also find a "single escape peak" in the spectrum. As an example, Fig. 13 shows the spectrum of pure ^{137}Cs radiation. In order to estimate the count rate, the (photon) peak needs to be integrated.

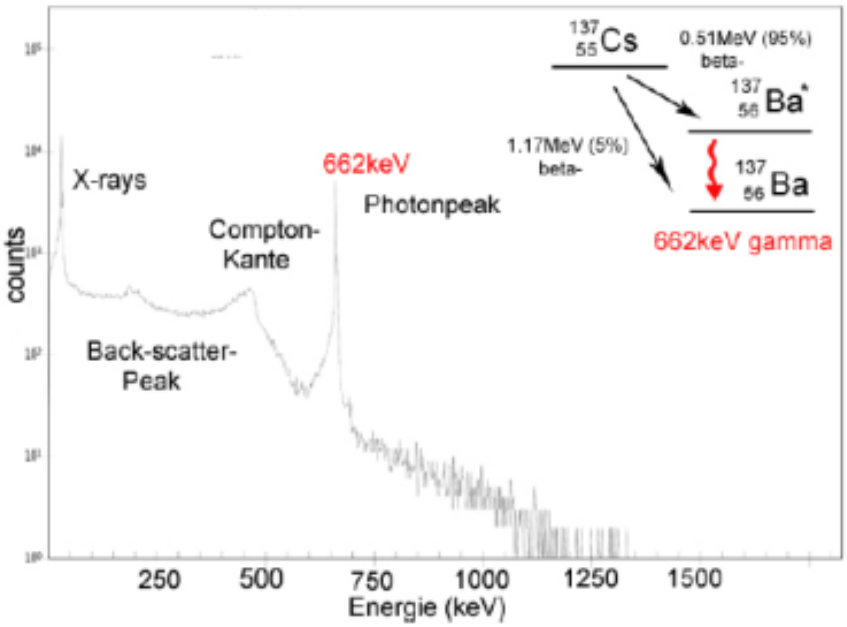

Figure 13: Spectrum and decay schematics of a pure ^{137}Cs source

3.3 RAD7 - a solid state α-detector system

The main source for the contents of this section is the user manual of the manufacturer (DURRIDGE Company Inc., 2020, see Appendix B2 for access). The RAD7 radon detector is a stand-alone field instrument for the measurement of radon activity concentrations in the range of several hundred to thousands Bq/m^3. It consists of a hemispheric measurement chamber of 0.7 litre and a semiconductor detector (Fig. 14 left panel). A high voltage power circuit charges the inside conductor to a potential of 2000 to 2500V, relative to the detector, creating an electric field throughout the volume of the cell. Filtered (i.e. radon progeny free) sample air containing the radon gases is flushed through the chamber where new radon daughters are formed. These daughters (^{218}Polonium from ^{222}Radon and ^{216}Polonium from ^{220}Radon, cf. Fig. 2) are normally positively charged and thus accelerated towards the detector where they stick. Since ^{218}Po and ^{216}Po are also unstable, they can decay on the detector's active surface emitting α-particles. With a 50% probability these α-particles enter the detector, generating an electric signal, which is proportional to its energy. Since the energies of the α-particles are characteristic for the different radon daughter isotopes, it is possible to precisely distinguish them.

An internal software evaluates the measurements. For each measurement the RAD7 saves the α–counts in different energy channels, named windows (A, B, C, D, Fig. 14 right panel). The RAD7 firmware offers different modes to determine the radon activity concentration. In SNIFF mode only the ^{218}Po signal is taken into account to determine fast changes of the ^{222}Radon activity concentrations. Because measurements are performed for less than three hours, SNIFF mode is used during manual ^{222}Radon flux measurement. Using the SNIFF mode, the typical sensitivity of the detector is 0.0067 cpm/(Bq/m^3). High air humidity reduces the sensitivity of the measurement, because the water molecules can neutralize the positively charged progeny before they arrive at the detector. According

to the manufacturer the humidity should be below 10%, therefore the air is (chemically) dried during the manual flux measurement.

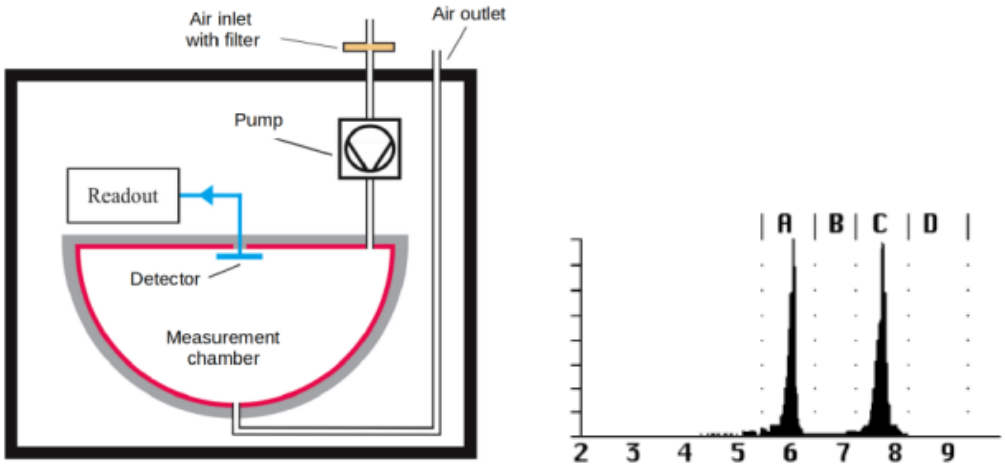

Figure 14, left: Schematic diagram of the RAD7 functionality (after Hoheisel, 2015). Right: Spectrum of the RAD7 where the x-axis corresponds to the α-energy and the y-axis to the number of counts (arbitrary units, from DURRIDGE, 2020; Appendix B2). The ^{218}Po (6.0 MeV) and ^{214}Po (7.69 MeV) counts (in approximate radioactive equilibrium = equal count rate) are shown.

The error of the activity concentration reported by RAD7 corresponds to the standard deviation of a Poisson distribution that is proportional to $\sqrt{N}$, N the number of counts. Since the Poisson distribution underestimates the error at low counting rates the RAD7 defines sigma as

$$\sigma = 1 + \sqrt{N + 1} \qquad (17)$$

and the reported value corresponds to 2σ.

3.4 AlphaGUARD - a pulse ionization chamber detector system

The following description is taken from the user manual provided by Bertin GmbH (Frankfurt Main, Germany, 2012), the manufacturer of the AlphaGUARD radon detector. This detector is applicable for radon activity concentrations in the range of hundreds to thousands of Bq/m^3; it uses the principle of a pulse ionization chamber. It detects individual ionizing events of the α-radiation of radon. The active volume of the stainless steel ionisation chamber has 0.56 liter with the outer walls of the measurement chamber lying on a potential of +750 V during measurement. The air sample with radon gas passes through a filter preventing radon daughter isotopes entering the active volume. In the measurement chamber α-particles from radon decay ionize air atoms and generate electron-ion pairs. An electric field forces these free charge carriers to move to the anode (electrons) or cathode (positive ions) (Fig. 15). There, they produce an electric pulse, which is measured. As the number of the electron-ion pairs is proportional to the energy of the α-particles, the measured current is proportional to the energy deposited per unit time in the ionization chamber. In the AlphaGUARD setting, it is possible to choose between a 1-minute and a 10-minute cycle. In our application where

we use the AlphGUARD as the radon detector in the automated flux chamber system *AutoFlux*, we use the 10-minute cycle.

According to the manufacturer, the 10-minute measurement cycle operates with a sensitivity of 1 cpm (count per minute) at 20 Bq m^{-3}. This means that one impulse corresponds to an activity concentration of 20 Bq m^{-3}. In contrast to the RAD7, the AlphaGUARD detector does not differentiate between different energy levels and can therefore not distinguish between different α-decays. Consequently, α-decay of ^{220}Rn and ^{222}Rn generate similar electric pulses. Also the positively charged radon daughters' (sticking on the cathode) decays are counted. This is a major disadvantage of the AlphaGUARD detector. In the AutoFlux system there is thus a delay volume built in, which allows the short-lived ^{220}Radon to decay before the air enters the AlphaGUARD.

The overall uncertainty of an AlphaGUARD measurement consists of different components (Rößler, Bertin, pers. comm. 2020): Due to the Poisson distribution of radioactive decay the uncertainty is proportional to the square root of the total number of ionization pulses. For example, an activity concentration of 300 Bq/m^3 measured over 10 minutes corresponds (as mentioned above) to 150 pulses; this yields a statistical error of $\sqrt{150}$ = 12.3 or 8%. A systematic error due to the calibration uncertainty must be considered in addition. New devices have a maximum systematic error of 3%, older ones an error of 5%. As the detector is not perfect, an additional factor has to be taken into account; this mainly concerns a linearity uncertainty of ca. 3%.

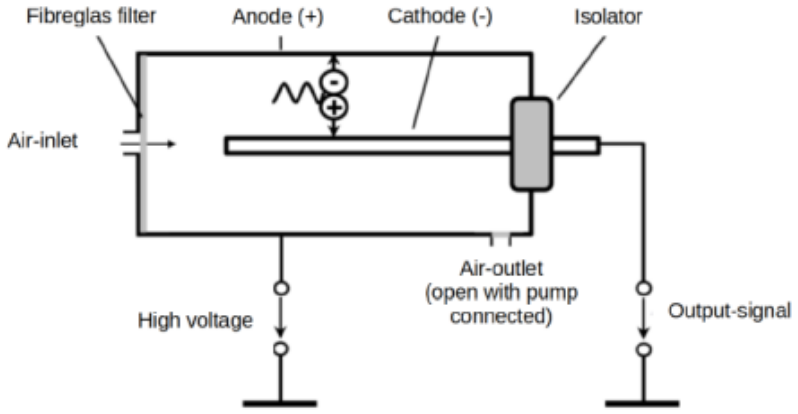

Figure 15: Schematic diagram of the AlphaGUARD detector system (after Rößler, 2019)

4 The Experiment

4.1 General remarks and time schedule

The advisor must be contacted well before the first day of the experiment to jointly organise the work. The first day then starts with a discussion to confirm the schedule and make sure that the basic theory and aims of the experiment as well as the used methods and instrumentation have been well understood. See also list of typical questions that the students should be able to answer (Appendix A1).

With kind support of the colleagues from the Heidelberg University Botanic Garden, all field measurements in this Experiment are conducted in the Botanic Garden (BG). On the first day, emphasis is laid on the field work there. **Please wear clothes and shoes which correspond to the respective outdoor conditions, and be aware that they could become also dirty especially under rainy conditions**. Manual radon flux measurements and soil core sampling for ^{137}Cs analysis are conducted there with subsequent first weighting for soil moisture analysis of 5 cm segments in the lab and drying of the soil samples overnight. We call this soil core *Cs-core*, but also one average ^{226}Ra analysis on the upper 20 cm of this core is performed four weeks later (after equilibration). Further, the AutoFlux data from the last days and weeks are inspected before the instrument is visited in the BG where also a second soil core is collected close-by. This core, which we call *texture-core*, is used for soil moisture and soil texture analysis only, the specific ^{226}Ra activity of the soil at this location had been determined earlier, i.e. during the original installation of the AutoFlux chamber. As done for the *Cs-core* the *texture-core* is also weighted for soil moisture analysis of 5 cm segments and the samples are dried overnight. After the field work, if not already on, the γ-detectors are started (see detailed instructions in Appendix A2), measurement and evaluation of the γ-spectra with the Genie 2000 software are briefly discussed and short test measurements are made to check the principal functioning of the detectors. A more detailed discussion will follow on the second day together with the energy calibrations of the detectors. To use all available measurement time, the detector efficiency measurement of the PGT detector is however started already on the first day (measurement overnight).

The second day is dedicated to a detailed discussion of measurement and evaluation of the γ-spectra with the Genie 2000 software. During/after the energy calibrations of the two detectors, the preparation of the dried *Cs-core* segments for γ-spectroscopy is made with the first segment measured immediately after the end of the energy calibration for ^{137}Cs at the PGT detector. On the DSG detector γ-measurement of ^{226}Ra progeny on an equilibrated *Cs-core* sample that was collected one month ago is started. After that, the finalised energy and efficiency measurements are evaluated. They will be used for all other γ-spectra. The measurement for efficiency calibration of the DSG detector is also already available. It had been conducted on the weekend before the current exercise. In the late afternoon or in the evening, the measurement of the 1st Cs sample is stopped (do not forget to save the spectrum) and the measurement of the 2nd Cs sample is started. In addition to the work on the γ-spectrometry, the texture analysis of the *texture-core* is also started.

On the third day, the texture analysis of the *texture-core* is continued, while here and on the next day γ-measurements of ^{137}Cs sample three and four (PGT detector) are continued. Further, the radon flux measurements with the AutoFlux system (and from the manual measurement) are evaluated.

On the fourth day, the 4rd *Cs-core* segment measured on the PGT and the ^{226}Ra progeny spectrum measured on the DSG detector are ended and evaluated. The termination of the samples has to be done before mid-day since at this time (Thursday at around 12 o'clock) the detectors are filled with

N_2 . After the filling of the detectors and the reheating of the electronic (e.g. + 40 min after the end of the N2 filling) an efficiency measurement with the Nussi standard is started (measurement over the weekend).

Table 1: Time schedule of the experiment

Day 1	- manual radon flux measurement in the Botanic Garden - soil core sampling for ^{137}Cs/^{226}Ra analysis (*Cs-core*) in the BG - inspection of ^{222}Rn flux measurements by AutoFlux - soil core (*texture-core*) sampling for soil texture analysis close to the AutoFlux - preparation of the *Cs-core* (soil moisture of 5 cm segments and drying) - preparation of *the texture-core* (soil moisture of 5 cm segments and drying) - short introduction to γ-spectroscopy - efficiency calibration of the PGT detector (overnight)
Day 2	- more detailed introduction to γ-spectroscopy - energy calibration of both detectors - preparation of the (dry) *Cs-core* for γ-spectroscopy (sieving, grounding) – γ-measurement of ^{137}Cs on 1. *Cs-core* segment with PGT detector - ^{226}Ra progeny measurement (until day 4) with DSG detector - evaluation of the energy and efficiency calibrations of both detectors - start of texture analysis of *texture-core* (two composite segments, 0-10 and 10-20 cm) - γ-measurement of ^{137}Cs on 2. *Cs-core* segment with PGT detector (overnight)
Day 3	- texture analysis of *texture-core* (two composite segments, 0-10 and 10-20 cm) – γ-meas. of ^{137}Cs on 3. *Cs-core* segment and evaluation of measured spectra - evaluation of radon flux measurements (manual and AutoFlux) - γ-measurement of ^{137}Cs on 4. *Cs-core* segment with PGT detector (overnight)
Day 4 & homework	– γ-meas. end of ^{137}Cs on 4. *Cs-core* segment and evaluation of spectra - evaluation of ^{226}Ra progeny spectrum from DSG detector, determination of specific ^{226}Ra activity of Cs-core and comparison with earlier measurements - start efficiency calibration measurement with Nussi standard at DSG detector - soil texture analysis finalised and evaluated - estimate of ^{222}Rn flux based on texture, soil moisture and ^{226}Ra content close to AutoFlux and comparison with direct flux measurements - preparation of composite sample (from 4 *Cs-core* segments 0-20 cm) for ^{226}Ra progeny equilibration and measurement > 4 weeks later - estimate of the total ^{137}Cs deposition in the Botanic Garden - discussion of the ^{222}Rn flux results from the Botanic Garden and comparison with earlier observations and with estimates from Karstens and Levin (2023)

4.2 Calibration of γ-detectors and evaluation of the spectra

For data acquisition and evaluation, the software “Genie 2000” (Canberra) is installed. Figure 16 gives a first overview of its functions.

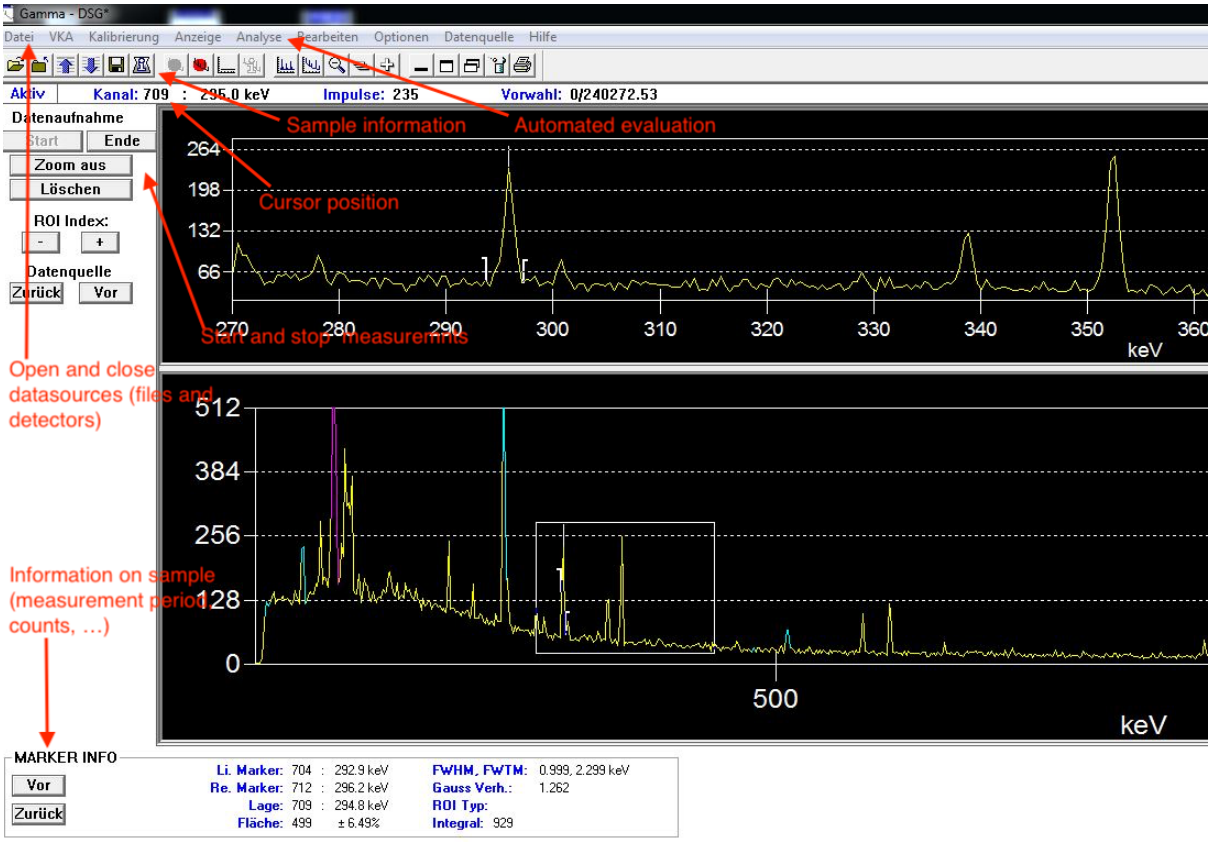

Figure 16: Display of the software "Genie 2000" with the γ-spectrum of an efficiency calibration of the DSG detector with the "Nussi" standard showing several nuclide peaks, including ^{226}Ra progeny; the upper panel shows a zoom of the channels enclosed by the rectangular in the lower panel

Tasks at IUP, basement day 1: efficiency measurement (overnight) of Eichstandard at PGT detector; day 2: energy calibration of both detectors, evaluation of efficiency calibration of both detectors, start of ^{226}Ra progeny measurement of equilibrated core sample from > 1 month ago at DSG detector; measurement of 1st and 2nd (overnight) Cs-core segment with PGT detector; day 3 and 4: continuation of Cs-core segment and of ^{226}Ra progeny measurements and evaluation of the spectra

4.2.1 Energy calibration of both detectors with ^{152}Europium source

γ-quants of the different energies are stored in the MCA, but in order to associate these channels with specific energies, a calibration is required. We use an ^{152}Europium source with a number of prominent γ-lines between 120 and 1500 keV for energy calibration.

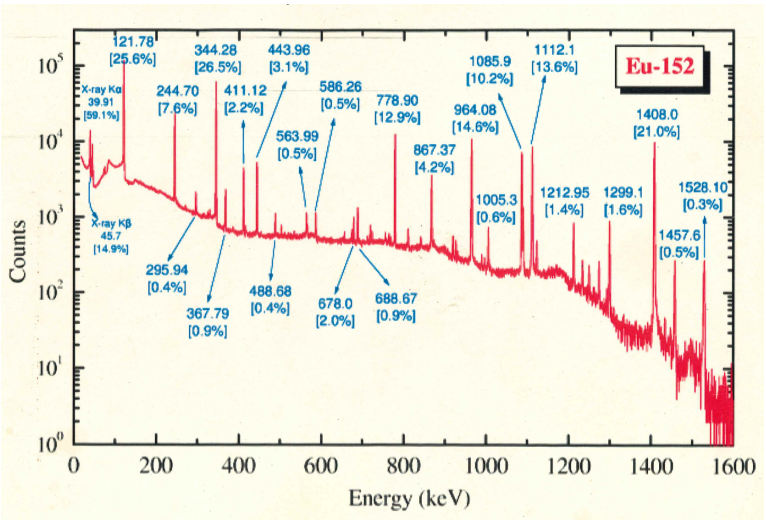

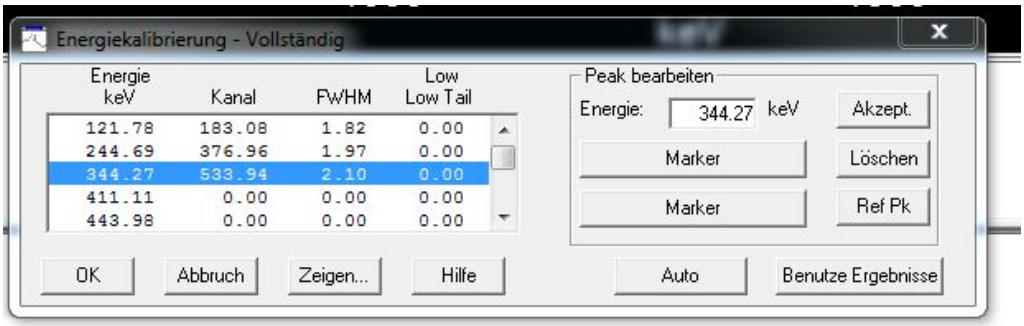

Figure 17: upper panel, γ-spectrum of ^{152}Eu; lower panel, Genie 2000 software showing the window for energy calibration with the ^{152}Eu source

Before we use the ^{152}Eu source, we roughly estimate the equivalent radiation dose from this source. ^{152}Eu is a β-emitter ($T_{1/2}$ = 13.5 a, 72% β^+, 28% β^-), but as the β-particles (and subsequent α-particles after β- decay) are absorbed in the shielding of the source, we have to account only for the γ-radiation. The activity of the source has recently (July 10, 2023) been determined to 2.005 kBq. The dose constant of ^{152}Eu is 0.124 mSv m^2 h^{-1} GBq^{-1}. Make realistic assumptions about the other parameters needed to apply Eq. 6 for equivalent dose rate estimate and compare your result with the dose rate calculator cited in Sec. 2 as well as with the mean natural equivalent dose for human population (cf. Fig. 1).

For the energy calibration of the detectors we put the ^{152}Eu source in front of the respective detector for around 10 min. Save ("sichern") the Eu-152 spectrum in a new directory, where all your spectra and calibration files are stored. The directory is created in the folder "C:\Benutzer\F56\2024\" and shall be named "date of directory creation_your two first names" The spectrum shall be named as follows: Detector name_date of directory creation_your two first names_Eu-152.CNF (e.g. DSG_20240201_MaxIngeborg_Eu-152.CNF). Then stop the measurement and open the just saved ^{52}Eu spectrum. Click menu entry "Kalibrierung -> Energie und Peakform" and the option "mit Nuklidliste" (Fig. 17, lower panel, the list of nuclides is "IUPBibliothek.NBL"). Choose ^{152}Eu from the drop-down list. Now a list of ^{152}Eu energies is shown and the corresponding channels of the selected peaks are read out of the measured spectrum using the cursor. To do so, mark the respective peak with a mouse left click and press the upper of the two "Marker" buttons. The respective channel is then introduced in the window. Press "Akzept." after each entry. (Alternatively, one can click "Auto" and the program

finds the channels automatically, but the entries must be checked also manually). A linear fit is calculated through the energy versus channel values, which can be displayed by choosing “Kalibrierung -> Energie zeigen”. After the energy calibration is finalised save (“sichern”) the calibration file in your new directory. The energy calibration file shall be named as follows: Detector name_date of directory creation_your two first names_Eu-152.CAL (e.g. DSG_20240201_MaxIngeborg_Eu-152.CAL). Finally, save again the Eu-152 and close the window.

4.2.2 Evaluation of the spectra

The measured spectra can be automatically evaluated with the Genie 2000 software. However, we first evaluate the spectra manually using the “Zoom” window and the cursors in the spectrum to mark the peak maximum and the baseline at the start and the end of the corresponding peak. With the option “Markerinfo” listed under the spectra we can read out the total integral under the peak and also the net counts (“Fläche”, here the background is subtracted). Also the “real” and the “live” time are listed in this window where the real time is corrected for dead time. For the automated evaluation we choose “Analyse” in the program. A compilation of the required steps has been stored under “Praktikum”. Further, there is an external Python script (on the gamma2024 computer in C:\Dokumente\fp\F56\programsanddata\GammRay\GammaRay.ipynb) for integration of the peaks. For the Python evaluation the spectra must be stored as *.TKA files together with the parameters of the energy-channel-relation. After the energy range of the peaks has been chosen, the Python script fits a Gaussian curve to each peak. All three results for the peak integration are compared and evaluated, taking into account the uncertainty of the three applied evaluation methods.

The activity of a sample is calculated from the counting rate, the abundance (*abn*), which gives the likelihood that a γ-quant is released during the specific decay and the efficiency (*eff*) of the detector at the energy of the decay to be evaluated

$$activity = \frac{counting \quad rate}{abn \cdot eff} \tag{18}.$$

The efficiency of the detector depends on the γ-energy and on the sample geometry. It is determined in this exercise for both detectors with the two different geometries for ^{137}Cs and ^{226}Ra progeny analysis. As standards with well-known activity are not available for all nuclides, which one may want to measure, the Genie 2000 software allows to determine an efficiency calibration curve. Two different calibration standards are used in our experiment, the standard “Nussi” for the ^{226}Ra (progeny) measurement on detector DSG and the so-called “Eichstandard” on detector PGT, which is used for the ^{137}Cs core measurements.

4.2.3 Efficiency calibration of DSG detector with Nussi standard

For the efficiency calibration of the DSG detector we use the standard “Nussi” from which we know the uranium content. This sample was prepared for an international comparison test between analytical geochemistry laboratories (Potts et al., 2003). Amongst the compared elements was uranium, which concentration in the sample was determined to (2.697 ± 0.186) mg/kg (Schwingshackl, 2013). The conversion factor from uranium concentration to ^{238}U activity concentration is taken from IAEA (1989), i.e. 12.35 Bq/kg per mg/kg uranium. The specific ^{238}U activity of the Nussi standard is, thus, 33.31 Bq/kg. Assuming radioactive equilibrium between ^{226}Ra and ^{238}U, the specific activity of ^{226}Ra would be the same, and this is also true for all its progeny in the sealed Nussi sample container.

Further taking into account the individual abundances of the up to 5 progenies we can use for the ^{226}Ra activity estimate of the soil cores as reported by Schkade et al. (2018) and listed in Tab. 1, we get the parameters for efficiency calibration of ^{226}Ra progeny measurement in the DSG detector. The efficiency calibration measurement with the Nussi standard had been conducted over the weekend before the exercise, to achieve good counting statistics of this low activity standard. Note that also the measurement of ^{226}Ra progeny is conducted in this exercise from the first to the fourth day to achieve good counting statistics on the *Cs-core* sample collected a month ago.

Table 1: Gamma lines used for DSG efficiency calibration with Nussi

Progeny	aktivity Bq/30g	energy keV	abundance %	
Pb-214	1.0	295.22	18.4	
Pb-214	1.0	351.93	35.6	(overlap with Bi-211)
Bi-214	1.0	609.31	45.5	
(Bi-214	1.0	1120.29	14.9)	
(Bi-214	1.0	1764.49	15.3)	

To calibrate the DSG detector for ^{226}Ra progeny measurement, open the γ-spectrum from the Nussi measurement conducted over the last weekend and choose “Kalibrierung -> Energie und Peakform -> mit Kalibrierdatei” to import the energy calibration. The calibration file is the one you created with ^{152}Eu for energy calibration. Determine the count rates of the individual nuclides in the Nussi γ-spectrum listed in Tab. 1 and enter the energy and efficiency values into the window (the latter are calculated manually from the count rate and the activity of the standard according to Eq. 18) using “Kalibrierung -> Effizienz -> durch Eingabe”. After the efficiency calibration is finalised save (“sichern”) the calibration file in your directory (cf. Section 4.2.1) as: Detector name_date of directory creation_your two first names_Nussi.CAL (e.g. DSG_20240201_MaxIngeborg_Nussi.CAL). Finally save the Nussi spectrum in the same directory as: Detector name_date of directory creation_your two first names_Nussi.CNF and close the window.

4.2.4 Efficiency calibration of PGT detector with Eichstandard

The efficiency calibration of the PGT detector based on the measurement of the Eichstandard follows the same steps as for the DSG detector. The calibration nuclides in the spectrum can be selected from the list in the right panel of Fig. 18 together with their expected activity at the reference date (April 1, 2011) of the standard. When calculating the efficiencies do not forget correcting for decay since April 1, 2011. The calibration and spectrum files are named as: Detector name_date of directory creation_your two first names_Cs-137Eich.CAL and CNF.

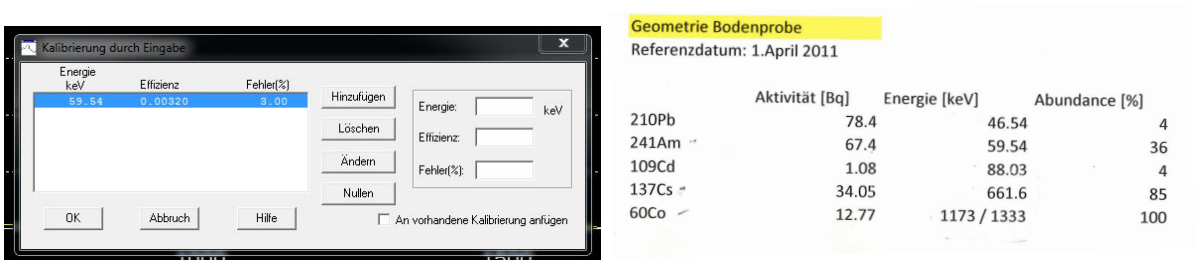

Figure 18: Efficiency calibration of the PGT detector with the nuclides in the Eichstandard

4.3 Soil core sampling and ^{222}Rn flux measurements in the Botanic Garden

All field measurements in this Experiment are conducted in the Botanic Garden (BG) of Heidelberg University. Here two fixed locations for manual respectively automated radon soil exhalation measurements are installed. Further, soil cores down to > 20 cm and 20 cm depth are collected for ^{137}Cs and ^{226}Ra activity concentration measurement as well as for soil moisture and texture measurements in the laboratory, respectively. **Note that soil cores are transported as undisturbed as possible in the coring device and in a plastic bag back to the IUP lab for accurate segmentation and soil moisture measurement.**

Task in BG (day 1: Manual measurement of radon exhalation rate with RAD7, Cs-core sampling):

4.3.1 Manual soil exhalation measurement

A stainless-steel frame has been permanently placed at an openly accessible location in the BG. Here manual measurements of the radon soil exhalation rate are conducted by covering the frame and accumulating exhaling gases in the soil chamber over the course of 1 hour. Chemically dried air from the chamber is circulated through a RAD7 detector and flushed back into the chamber. A schematic of the manual chamber setup is displayed in Fig. 19. The outlet tubing at the chamber top is connected via a drying cartridge and a filter to the inlet of the RAD7. The outlet of the RAD7 is connected back to the inlet tubing of the chamber. Then the chamber top is put on the frame and sealed with water in the rim of the stainless-steel frame. 10-minute mean activity measurements (Sniff mode) are conducted over one hour. From the volume of the chamber (V = H * A, **do not forget to measure the height of the chamber**), plus the volume of the tubing, the drying cartridge and the RAD7 chamber, the surface covered by the chamber and the measured ^{222}Rn increase over one hour the exhalation rate is calculated according to Eq. 19.

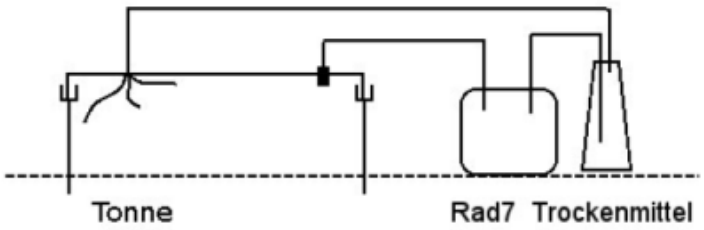

$$j = \frac{\Delta C(t)}{\Delta t} \cdot \frac{V}{A} \qquad (19)$$

Figure 19: Schematic setup of the manual radon flux measurement (from Hoheisel, 2015)

4.3.2 Soil core sampling at a (random) location in the BG Arboretum for ^{137}Cs and ^{226}Ra

While the radon increase in the (manual) chamber is measured, a soil core (*Cs-core*) is collected. In order to resolve a ^{137}Cs profile in the soil with a peak of the Chernobyl fall-out, an undisturbed location (at least since the year of the accident in 1986) is required. A typical profile as was measured in 2010 close to Heidelberg is shown in the right panel of Fig. 20. The distribution of total ^{137}Cs depositions in an area of about 25 km around Heidelberg is displayed in the left panel. Today, about 15 years later, we expect the ^{137}Cs maximum further down, i.e. around 5-15 cm depth, as Cesium is bound to organic material and therewith transported into deeper layers of the soil. We choose a place in between the high old trees in the Arboretum of the Botanic Garden, where we expect - as much as possible - undisturbed soil conditions. **Note that only selected lawn areas are allowed for our sampling, concerning only regions where the grass is regularly cut during the vegetation period. Other areas must not be disturbed in order to protect the ecosystem (insects, soil organisms, etc.).**

Figure 20: Left: Distribution of ^{137}Cs deposition about 25 km around Heidelberg (data from Dörr and Münnich, 1987). Right: Soil profile of ^{137}Cs as measured in 2010 at the Heiligenberg, close to Heidelberg.

Successive tasks at IUP (day 1: First weighting for soil moisture measurement on 5 cm segments of the Cs-core (see Sec. 4.4); day 2: Second weighting for soil moisture and preparation for ^{137}Cs measurement (sieving and grounding), see laboratory instructions below).

4.3.3 Automated soil exhalation measurement and soil core for moisture and texture analysis

In a closed area of the BG, which is only accessible with special permission, an automated system for the quasi-continuous measurement of the radon exhalation rate from the soil has been installed (AutoFlux, see Fig. 21). A detailed description of the instrument is available in the AutoFlux manual (see Appendix B1 for access). The instrument's power supply (12 V) comes from a solar panel. The Raspberry Pi of the system (RPi5) is programmed to regularly close (and open) the chamber every 3 hours for a 1-hour accumulation of radon exhaled from the soil surface. It automatically transfers the 10-minute average radon activity concentrations measured with an AlphaGUARD (AG) and stored on a data logger to a directory in the HeiBox (https://heibox.uni-heidelberg.de/library/b93f8943-6799-

4368-95ae-9ba771f89cdc/Radon/Test/). In addition to radon, also 10-min averages of the air flow rate through the AG, air temperature, pressure and humidity, rainfall and soil temperature and humidity in the upper 10 cm of the soil under the chamber are measured, logged and transferred to the HeiBox. The RPi5 is remotely connected via WLAN router and accessible via TeamViewer.

Tasks at IUP basement (day 1: Check AutoFlux measurements of the last weeks):

Download the 10-min data of the last and current month from the HeiBox and check the proper functioning of the AutoFlux during the past weeks (flow rate and measured data).

Tasks in Botanic Garden (day 1: Visit AutoFlux in BG, collect texture-core):

Check the AutoFlux physical appearance, clean the upper edge of the chamber and the movable top from dirt. If required, adjust the flow rate.

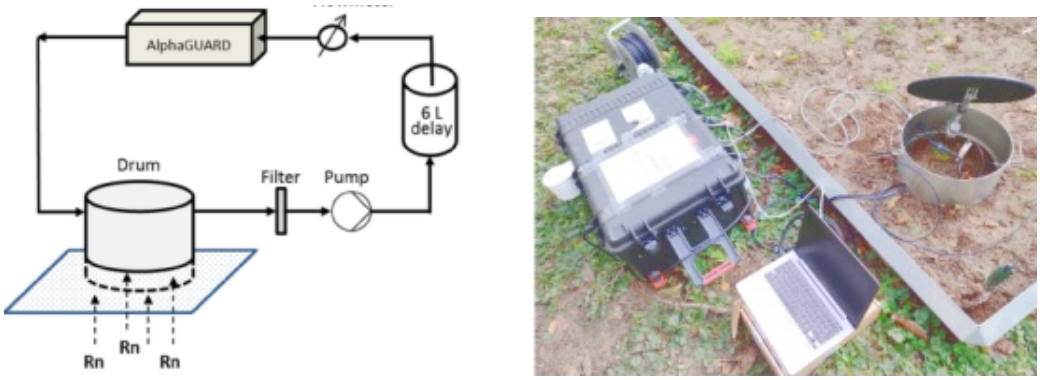

Figure 21: Schematic flow diagram and photograph of the AutoFlux system (Photo from Jandl, 2021; for details see also AutoFlux manual, Appendix B1)

Collect a soil core down to 20 cm (go not deeper since there are a lot of gravels below!) in the immediate surroundings of the AutoFlux chamber (to sample similar soil as is under the chamber).

Successive tasks in IUP lab (day 1, 2,3 & 4: prepare texture-core for, and determine soil moisture, porosity and texture, for details see laboratory measurements, Sec. 4.4)

4.4 Laboratory measurements

4.4.1 Physical properties of the soil cores

Soil moisture is measured on both soil cores on 5 cm segments (measured from the soil surface downwards) by weighting before and after drying (overnight) of the individual segments at 105°C. It is important, particularly in summer, to keep the soil core as undisturbed as possible in the metal

coring mantle until it is cut in the laboratory. Before cutting, make a photograph of the entire core and note possible layering as indicated by color change or visible texture differences. Possible (green) grass is carefully removed from the top of the core before segmentation. Important: try to avoid any loss of moisture from the open soil sample before first weighting of the (wet) core segments.

Most important for texture core: In order to accurately determine the bulk density and porosity of the soil sample, it is important to cut the core into exactly 5 cm segments. Together with the known diameter of the core (5.7 cm) we calculate the volume of the segment and can estimate the bulk density of the core, assuming that the structure of the soil core has not been destroyed during core sampling. Further, with the density of the solid soil material (ca. 2.65 g cm^{-3} for quartz/sand) we can estimate the porosity of the soil (important to calculate the ^{222}Rn flux, cf. Eq. 13). The density of the soil material is determined by mixing a certain mass of dry soil with water and measuring the volume of the suspension in an Erlenmeyer flask or measurement cylinder (see 4.4.4).

Tasks in IUP lab (day 1: segmentation of the freshly collected Cs-core and texture-core, first weighting for soil moisture)

The wet segments of the core are put into aluminum dishes and are weighted; they are carefully broken-up before drying (sieving will be difficult if dried clay crumbles strongly stick together). Make sure to clearly mark all 5 cm segments in order not to confuse the sequence of the core (counted downwards from the soil surface). The *Cs-Core* and its samples are named "BGL-xx" and "BGL-xx-yy", respectively, with xx a running number over all collected cores within FP56 (will be communicated by the adviser) and yy numbers from 1 to 4 core downwards. The *texture-Core* and its samples are named accordingly "BGA-xx" and "BGA-xx-yy". Samples are dried overnight at 105°C (oven in room 528) and weighted again the next day, the difference between wet and dry soil sample is the soil moisture. Soil moisture is often reported as percent saturation S (cf. Eq. 9, with S = 100% meaning that the entire pore space, the porosity θ_p is filled with water) or in percent of the **total** soil volume θ_w (note that $\theta_p + \theta_S = 1$ with θ_S the percentage of the volume filled with soil grains). The *texture-core* is further analysed for soil texture (see below), while the dry *Cs-core* segments are directly prepared for γ-spectroscopy of ^{137}Cs.

Tasks in IUP lab (day 2: second weighting for soil moisture, sieving and grounding of Cs-core segments, preparation for ^{137}Cs γ-spectroscopy.)

4.4.2 Preparation of *Cs-core* segments

After drying of the sample segments, roots and pieces of wood (i.e. the organic fraction) are removed from the samples. The rest of each segment is sieved to remove particles > 2 mm (gravel fraction). The sieved fractions are grounded/homogenized and filled into dedicated plastic boxes for ^{137}Cs spectroscopy (same size and geometry as the Eichstandard used for efficiency calibration, Sec. 4.2.1). The net sample weights are determined (to later calculate the specific activity of the sample in Bq/kg soil material).

From day 2 on, *Cs-core* segment are measured in the PGT detector for 12h each. Make sure that the positions of the sample boxes are exactly at the same place as that of the Eichstandard.

After all ^{137}Cs measurements on the *Cs-core* have been finalised (i.e. on day 4 of the Experiment), aliquots from the four sample segments of the upper 20 cm are mixed together and prepared for ^{226}Ra progeny analysis (one month later). For the composite sample (named as "BGL-xx-00-20cm") 25% (by weight) of each 5 cm segment are put together, carefully mixed and the composite sample is transferred into a dedicated container for the ^{226}Ra progeny measurement (same size and geometry as the Nussi standard). The sample is weighted and carefully sealed. When filling the container, it is important to carefully protect the O-ring and the screw holes (use transparent adhesive scrip) during the sample transfer. In addition, it is absolutely mandatory to the seal the sample for ^{226}Ra progeny measurement air-tight so that no ^{222}Rn, the only gaseous progeny of ^{226}Ra (cf. Fig. 2) can escape during the one-month storage period during which all progeny come into radioactive equilibrium with the ^{226}Ra in the soil sample.

Tasks in IUP lab (day 2 – analysis of texture-core: second weighting for soil moisture estimate, sieving and measurement of porosity (Sec. 4.4.4), and preparation for grain size distribution measurement (Sec. 4.4.5))

4.4.3 Preparation of *texture-core* segments

The procedure for preparation of the *texture-core* for soil moisture determination is principally the same as for the *Cs-core*, however, after separate drying and weighting of the four 5 cm segments the upper and the lower two segments are mixed together into one sample each (then we have only two samples, 0-10 cm and 10-20 cm named "BGA-xx-00-10cm" and "BGA-xx-10-20cm" for further analysis). On these two samples we determine not only the density of the soil material for the porosity measurement, but also its grain size distribution, which is needed to estimate the emanation rate of radon from the soil grains (cf. page 6). After removing the organic material, samples are sieved to separate the gravel fraction (> 2 mm). The portions of the gravel and <2mm fractions are noted, and 25 g of all sieved fraction are transferred into an Erlenmeyer flask for soil porosity, and into a beaker glass for grain size distribution measurements, respectively.

4.4.4 Determination of soil porosity

If we were able to collect a soil core that has kept its original structure during coring, the total volume of each core segment is known. The dry bulk density ρ_b can then be determined from the dry mass of the dry soil m_{soil} and the total volume V of the core segment:

$$\rho_b = \frac{m_{soil}}{V} \qquad (20)$$

We can then determine the porosity θ_P if the density of the soil material ρ_s is known according to

$$\rho_b = \rho_s (1 - \theta_P) \qquad (21)$$

The density of the soil material ρ_s is measured as follows: The 25 g of dry (sieved) soil material in the Erlenmeyer flask is flushed from the walls to the bottom of the flask with about 50 ml of distilled water. This mixture is heated for about 10 min and then slightly shaken to remove air bubbles from

the suspension. After cooling of the suspension to room temperature (ca. 2 hour), the Erlenmeyer flask is filled with distilled water up to a total volume of exactly 100 ml and the suspension is weighted. The weight of the share of water in the 100 ml suspension is calculated as

water = total weight – 25 g soil – weight of the Erlenmeyer flask

Assuming a water density of 1 g/cm^3, we can calculate its volume share in the 100 ml suspension and further the volume of the 25 g of soil. This allows calculating ρ_S and with Eq. 21 the porosity of the soil segment.

4.4.5 Determination of grain size distribution

In our experiment we determine the grain size distribution, which we need to know for estimation of the ^{222}Rn emanation from the soil grains (Eq. 8) by hydrometer analysis (after Gandahl, 1953, see also http://publications.iodp.org/proceedings/308/205/205_4.htm). In soil science we distinguish the following soil fractions:

gravel: d > 2 mm (was already removed by sieving)
sand: 63 μm < d < 2 mm
silt: 2 μm < d < 63 μm
clay: < 2 μm

The hydrometer analysis applies Stokes's law, which governs the terminal velocity at which spherical particles settle through a column of fluid. Stokes's law assumes particles that (1) are rigid, spherical, and smooth; (2) have similar density; (3) are separated from each other; (4) do not interact during sedimentation; and (5) are large enough so that settlement is not governed by Brownian motion. Stoke's law is also strictly only applicable to slow fluid movements that display laminar flow patterns (i.e., Reynolds number = <1). These properties are generally not valid for soil particles, nevertheless, the hydrometer analysis is often applied in soil science and also in oceanography to characterise ocean sediments.

Hydrometer analysis begins after thoroughly mixing the soil material and water, after which particles settle out of the water column according to Stokes's law. The density of a sediment-water suspension depends on the concentration and specific gravity of the sediments present in the mixture. If the suspension is allowed to stand, particles will settle out of the suspension and the density of the sediment-water suspension will decrease. A hydrometer measures the density of the suspension at a known depth below the surface.

Tasks in IUP lab (day 2 – prepare sample for grain size distribution measurement)

- If necessary, the soil has to be purified from salts and humus.
- 25 g dry soil (particles passing sieve 2 mm, see 4.4.2) is transferred into an beaker glass
- 100 ml 0.05 molar solution of sodium hexametaphosphate ($(NaPO_3)_6$, preparation of the solution, see Appendix A3) and another 50 ml of distilled water are added and stirred carefully for several minutes to make it homogeneous, the soil material must be fully suspended in the solution.
- After stirring, the spoon is cleaned with distilled water to transfer all soil material into the solution. The suspension is kept for at least 2 hours (better is however overnight) in the beaker

glass (covered with Parafilm). Shake the beaker glass from time to time to accelerate the suspension of the soil material.

Tasks in IUP lab (day 3 – conduct first part of grain size distribution measurement)

After 24 hours, the suspension is again thoroughly stirred and then transferred into a measurement cylinder. Carefully clean the rod and glass and make sure all soil grains are transferred. Then add distilled water to the suspension to fill it up to 1000 ml. A second 1000 ml cylinder is filled with reference solution (i. e. without soil). Now the hydrometer measurements can start.

- Cover the cylinder with Parafilm and turn it upside down 10 times
- Start the stop watch
- After 90 sec put hydrometer into the solution
- After 120 sec, carefully read out hydrometer (to 4 decimal places) at the surface of the solution (at this point in time all particles < 63 μm are still suspended)
- Let the cylinder (with hydrometer) stand for another 24 hours
- Make temperature and hydrometer measurement in the reference solution

Tasks in IUP lab (day 4 - grain size distribution measurement finalised)

- After 24 hours, carefully read out again hydrometer (to 4 decimal places) at the surface of the solution (at this point in time all particles < 2 μm are still suspended)
- Make again temperature and hydrometer measurement in the reference solution.

4.5 Evaluation of measurement results (day 3, 4 and home work)

4.5.1 Transfer of AutoFlux data from the HeiBox and their evaluation

All 10-minute AutoFlux measurements are automatically transferred to a directory of the HeiBox (https://heibox.uni-heidelberg.de/library/a5d2a132-504c-4b7c-82e9-5ce02d1632ba/FPraktikum/Datenuploads/Radon/Test). There is a python script available (on the gamma2024 computer in C:\Dokumente\fp\F56\programsanddata\Autoflux\read_data_V2.ipynb) that allows to evaluate these data and estimate hourly mean ^{222}Rn fluxes from the activity concentration increases while the chamber is closed (i.e. from 0:00 – 1:00, 3:00 – 4:00, etc., times in UTC, indicated in the file by "1" in the column "Activity"). The first measurement at the start of the hour is discarded. The program calculates linear regressions through the remaining 5 data points of the hour. It also allows to plot all other measured parameters (air temperature, humidity and pressure, soil temperature and moisture from 0-10 cm, rain fall).

As mentioned already in Sec. 4.3.3, before visiting the AutoFlux in the Botanic Garden, the data of the last weeks are downloaded and the temporal variations of all parameters during the last week is plotted. Use the directory C:\Dokumente\fp\F56\Temp on the gamma2024 computer to visualize the data. The values are checked for plausibility. Particularly important is the flow rate through the entire system incl. AlphaGUARD, which often decrease if atmospheric humidity is high. During the home work, the data of at least the last month are evaluated and mean values of the ^{222}Rn flux and its variability are evaluated.

4.5.2 Estimation of the ^{222}Rn flux from the manual measurement on day 1

The RAD7 stores all measurements of the last months, they can be read out manually from the instrument. Equation 19 then allows to calculate the flux from the temporal ^{222}Rn increase and the total volume and surface area of the chamber. The results are compared with the data from the AutoFlux and with already existing data from RAD7 measurements (reported in the file "Botanicgarden.xlsx"). Discuss the reasons for possible differences.

4.5.3 Estimation of the ^{222}Rn flux from measured ^{226}Ra, soil porosity, grain size distribution and soil moisture

Estimating the ^{222}Rn flux from bottom-up soil parameters is described in detail in Sec. 2.2. Follow the corresponding equations using the parameters measured on the *texture-core*. The specific ^{226}Ra activity is assumed to be aa ± bb Bq/kg (value will be communicated by the adviser), i.e. the same as measured in the soil core under the AutoFlux chamber. To estimate the uncertainty of this ^{222}Rn flux calculation, consider (1) the error of the ^{226}Ra activity, (2) the uncertainty of the porosity estimation arriving from a filling error of 0.5ml in the Erlenmeyer flask and a weighting error of 0.1g, and (3) the error of the grain size distribution measurements arriving from the hydrometer uncertainty of 0.0002 g cm^{-1} . Which uncertainty dominates?

4.5.4 Comparison of ^{222}Rn fluxes estimated from observations in the Botanic Garden with earlier observations and modelled fluxes

Karstens and Levin (2023) published European-wide estimates of the ^{222}Rn exhalation rate based on maps of soil Uranium, soil texture and soil moisture that was modelled with land surface models based on meteorological data. Their estimated monthly (2008 – 2019) and daily fluxes (2017 only) for the region around Heidelberg are displayed in Fig. 22, together with the modelled air-filled soil volume. The model results of the air-filled soil volume are compared with observations at Grenzhof (west of Heidelberg, a station where soil moisture had been continuously monitored in earlier years). Modelled ^{222}Rn fluxes are compared with observations from sites in the Neuenheimer Feld and Heddesheim published by Schwingshackl (2013). Also a climatology of ^{222}Rn fluxes based on long-term measurements from south of Heidelberg (see Karstens et al., 2015) are included in the comparison.

Discuss your ^{222}Rn flux and soil moisture measurements in the Botanic Garden in the context of the earlier data (see file "Botanicgarden.xlsx") and model results displayed in Fig. 22. Do your results fall into the range of model results for the Heidelberg area and the specific time of the year? What are the main uncertainties in your observation-based estimates? What could be reasons for discrepancies between observations and model? Discuss the representativeness of your measurements. Also compare your measured soil texture and ^{226}Ra data with those used in the calculations of Karstens and Levin (2023). Which information is required to scale up point measurements and make them more representative?

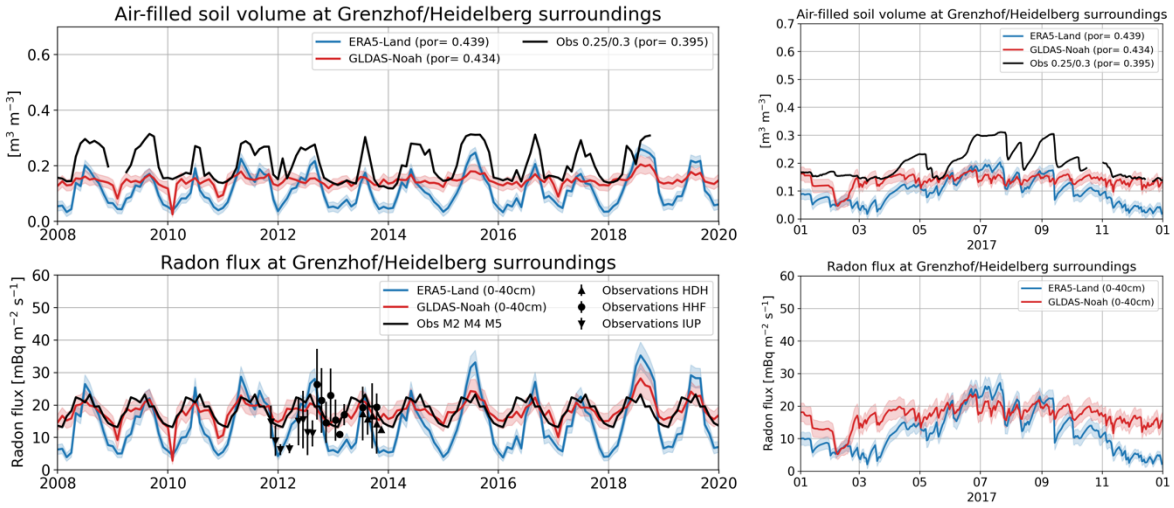

Figure 22: Time series of observed and modelled air-filled soil volume (upper panels) and modelled and monthly means from sporadically measured radon fluxes (lower panels) for sampling sites around Grenzhof and Heidelberg, Germany. The solid black line is the observation-based climatology calculated from long-term flux measurements conducted in the 1980s and 1990s at three sites south of Heidelberg.

4.5.5 Estimation of the total ^{137}Cs fall-out from Chernobyl in the Botanic Garden

From the specific ^{137}Cs activities in the 5 cm segments the total ^{137}Cs "standing crop" (i.e. the current inventory per m^2) in the upper 20 cm of the soil is calculated. Compare the result with the data from Dörr and Münnich (1987) displayed in Fig. 20 (left panel) by correcting for decay since 1987 (the radioactive life time of ^{137}Cs is 43.5 years). Calculate the vertical profile of the relative share of ^{137}Cs in your core and compare with the profile observed about 40 years ago. What is your guess how much ^{137}Cs already reached soil depths below 20 cm?

4.5.6 Final discussion on the use of point measurements and their extrapolation to larger areas

Discuss the general limitations of point measurements in environmental science and their representativeness for larger areas.

Appendices

A1 Questions to be answered before starting the Experiment

- What is the main aim of the Exercise?
- What are the categories of radioactive isotopes and which are their sources?
- Which processes/isotopes contribute most to the mean radiation dose of human population?
- What are the functionalities of radiation detectors, where do we use γ-spectroscopy, what is the advantage compared to α-or β-detection?
- Why are γ-detectors permanently cooled?
- Describe a typical γ-spectrum
- What are the steps of a detector calibration, what do we need to know?
- What is the origin of atmospheric radon?
- Why do we distinguish indoor and outdoor radon?
- Describe a simplified ^{222}Rn profile in the unsaturated soil zone?
- What are the parameters for estimation of the ^{222}Rn flux into the atmosphere?

A2 Starting of γ-detectors

The γ-detectors used in this exercise are very sensitive instruments and must not be started in absence of the supervisor. It is important to slowly increase the high-voltage power supply, otherwise there could be serious damage on its electronic components!

- Before start of the γ-detectors, make sure these have been cooled down with liquid nitrogen (-196 °C) over the last three weeks (2 x weekly re-fill of the Dewar containers).
- Put the ^{152}Europium source in front of the detector to have a g-source. In order to watch the signal from the pre-amplifier, connect the output of the amplifier in the electronic rack via BNC cable with one channel of the oscilloscope.
- Before switching on the power supply of the electronic rack, make sure both high-voltage switches are in the off-position and the potentiometers are at zero.
- Then switch on the high-voltage switch and slowly increase the voltage with the potentiometer in steps of 0.1 kV. After each step, we observe a short decrease of the signal and finally the noise-free total signal.
- Note that the final voltage of the DSG detector is 1 kV while that of the PGT detector is at 3 kV.

During the semester, when one exercise follows the next, the high-voltage is not switched off but the detectors are kept running. This is better than frequently switching on and off. Before switching off the detectors, decrease the voltage (not as slowly as during switching on). The power supply of the detector systems runs over an UPS (uninterruptable power supply) to avoid fast on-off if power supply is interrupted.

A3 Preparation of the sodium hexametaphosphate solution to measure grain size distribution

15 g of sodium-hexametaphosphate ($(NaPO_3)_6$ are dissolved in 300 ml of distilled water (baker glass, stir until all crystals are in solution). Take 105 g of this solution to prepare one soil sample of 25 g for grain size analysis with the hydrometer (Sec. 4.4.5).

B1 Manual of the AutoFlux system

Please download the file “AutoFlux_ATTO_forFP56exported.pdf” at https://heibox.uni-heidelberg.de/library/b93f8943-6799-4368-95ae-9ba771f89cdc/Radon/Manuals. A printed version will be also available during the experiment.

B2 Manual of the RAD7 detector

Please download the file “RAD7_Manual.pdf” at https://heibox.uni-heidelberg.de/library/b93f8943-6799-4368-95ae-9ba771f89cdc/Radon/Manuals or at https://durridge.com/documentation/RAD7%20Manual.pdf . A printed version will be also available during the experiment.

References

Bossew, P.: Radon priority areas – definition, estimation and uncertainty. In: Nuclear Technology & Radiation Protection 33, 3, 286–292, 2018, http://doi.org/10.2298/NTRP180515011B.

Cinelli, G., De Cort, M. & Tollefsen, T. (Eds): European Atlas of Natural Radiation, ISBN 978-92-76-08259-0, https://data.europa.eu/doi/10.2760/46388, 2019.

Dörr, H. and Münnich, K.O.: Spatial distribution of soil- ^{137}Cs and ^{134}Cs in West Germany after Chernobyl. Naturwissenschaften 74, 249-51, doi: 10.1007/BF00424599, 1987.

European Union. Council Directive 2013/59/Euratom of 5 December 2013 laying down basic safety standards for protection against the dangers arising from exposure to ionising radiation etc., http://eur-lex.europa.eu/legal-content/EN/TXT/PDF/?uri=OJ:L:2014:013:FULL&from=EN, 2013.

Faure, G. and Mensing, T.: Isotopes - principles and applications. John Wiley and sons, 2005

Karstens, U., Schwingshackl, C., Schmithüsen, D., and Levin, I.: A process-based ^{222}radon flux map for Europe and its comparison to long-term observations, Atmos. Chem. Phys., 15, 12845– 12865, https://doi.org/10.5194/acp-15-12845-2015, 2015.

Karstens, U. and Levin, I.: Update and evaluation of a process-based radon flux map for Europe (V1.0). ICOS RI, https://hdL.handle.net/11676/8PqEdm7ARD6aPepClmktPm2K, 2023.

IAEA: Construction and Use of Calibration Facilities for Radiometric Field Equipment, International Atomic Energy Agency, Vienna, Austria, Technical Reports Series 309, 86 pp., 1989.

Jandl, I.: ^{222}Rn exhalation from soils: Field deployable profile measurement techniques in soil and characterization of an automated measurement system for continuous ^{222}Rn flux observations at the soil surface. Bachelor thesis, Institut für Umweltphysik, Heidelberg University, 63 p., 2021.

Levin, I., Born, M., Cuntz, M., Langendörfer, U., Mantsch, S., Naegler, T., Schmidt, M., Varlagin, A., Verclas, S., and Wagenbach, D.: Observations of atmospheric variability and soil exhalation rate of Radon-222 at a Russian forest site: Technical approach and deployment for boundary layer studies, Tellus, 54B, 462–475, 2002.

Levin, I., Karstens, U., Hammer, S., DellaColetta, J., Maier, F., and Gachkivskyi, M.: Limitations of the radon tracer method (RTM) to estimate regional greenhouse gas (GHG) emissions – a case study for methane in Heidelberg, Atmos. Chem. Phys., 21, 17907–17926, https://doi.org/10.5194/acp-21-17907-2021, 2021.

Millington, R. J. and Quirk, J. P.: Transport in Porous media, Proceedings of the 7th International Congress of soil Science, Madison, Wisconsin, USA, 97–106, 1960.

Nazaroff, W.: Radon transport from soil to air, Reviews of Geophysics, 30, 137-160, 1992.

Porstendörfer, J.: Tutorial/Review: Properties and behaviour of Radon and Thoron and their decay products in the air, Journal of Aerosol Sciences 25(2), 219–263, 1994.

Potts, P. J., Thompson, M., Chenery, S. R., Webb, P. C., and Kasper, H. U.: GeoPT13 - An international proficiency test for analytical geochemistry laboratories - report on round 13/July 2003 (Köln Loess). *International Association of Geoanalysts*, 2003.

Schery, S. D. and Wasiolek, M. A.: Radon and Thoron in the Human Environment, chap. Modeling Radon Flux from the Earth's Surface, 207–217, World Scientific Publishing, Singapore, 1998.

Schkade, U.-K., Heckel, A. and Wershofen, H.: Gammaspektrometrische Bestimmung der Aktivitäten natürlicher Radionuklide, Budesamt für Strahlenschutz & Physikalisch-Technische Bundesanstalt, ISSN 1865-8725, 2018.

Schüßler, W.: Effektive Parameter zur Bestimmung des Gasaustauschs zwischen Boden und Atmosphäre, Ph.D. thesis, Heidelberg University, Germany, 1996.

Schwingshackl, C.: Experimental Validation of a Radon-222 Flux Map, Master Thesis, Institut für Umweltphysik, Heidelberg University, Germany, 100 pp., 2013.

Strahlenschutzkommisson: 20 Jahre nach Tschernobyl - Eine Bilanz aus Sicht des Strahlenschutzes / Bundesministerium für Umwelt, Naturschutz und Reaktorsicherheit. 2006 (50). Forschungsbericht.

Stull, R.: An Introduction to Boundary Layer Meteorology. Kluwer Academic Publishers, pp, 1998.

Wichmann, H. E., Menzler, S., Schaffrath-Rosario, A., and Kreienbrock, L., Lung Cancer Risk in Germany Attributable to Radon in Homes, Epidemiology 17(6), S68-S69, 2006.

Zhuo, W., Guo, O., Chen, B., and Cheng, G.: Estimating the amount and distribution of radon flux density from the soil surface in China, J. Environ. Radioactiv., 99, 1143-1148, 2008.